In: Mathematical Methods and Models
Editor: Alain Miranville, pp. 1-41
ISBN 1-59454-317-8

Chapter 1

PHASE SEPARATION IN STOCHASTIC CAHN-HILLIARD MODELS

Dirk Blömker[*]
Institut für Mathematik, Templergraben 55
RWTH Aachen, 52062 Aachen, Germany
Stanislaus Maier-Paape[†]
Department of Mathematical Sciences
George Mason University
Fairfax, VA 22030, USA
Thomas Wanner[‡]
Department of Mathematical Sciences
George Mason University
Fairfax, VA 22030, USA

Abstract

The Cahn-Hilliard equation is one of the fundamental models for phase separation dynamics in metal alloys. On a qualitative level, it can successfully describe phenomena such as spinodal decomposition and nucleation. Yet, as deterministic partial differential equation it does not account for thermal fluctuations or similar random effects. In this survey we describe some dynamical aspects of a stochastic version of the model due to Cook. These include recent results on spinodal decomposition, as well as a brief discussion of nucleation and its relation to the deterministic attractor structure. In addition, differences between the deterministic and the stochastic dynamics are discussed.

[*]E-mail address: bloemker@instmath.rwth-aachen.de
[†]E-mail address: wanner@math.gmu.edu
[‡]E-mail address: wanner@math.gmu.edu

AMS Subject Classification: 60H15, 35K35, 35B05, 35P10

Keywords: stochastic Cahn-Hilliard equation, pattern formation, spinodal decomposition, nucleation

1 Introduction

Phase separation phenomena in composite materials have drawn considerable interest over the past few decades. Part of this interest can certainly be attributed to the wealth of intricate phenomena which can be observed. Yet also the prospect of more or less immediate implications for the design of new materials plays a significant role. One important aspect of such design questions is the stability or instability of the composite material in the following sense. Many composites are formed by combining materials which would not occur naturally within a compound. On the one hand, this fact is responsible for obtaining materials which exhibit novel and highly desirable properties. On the other hand, this artificial combination of the components can cause problems. In many cases, the composite material has to be used under service conditions, under which its components tend to separate, i.e., the alloy exhibits some form of instability. Traditionally, one distinguishes between two different instability mechanisms:

- **Spinodal Decomposition:** If all the components of a metal alloy are heated to a sufficiently high temperature, they quickly form an almost perfect homogeneous mixture. If this mixture is rapidly quenched to a low temperature, the solution solidifies and a process of phase separation may set in. The components start to separate again, thereby forming a highly inhomogeneous fine-grained structure with snake-like patterns exhibiting a characteristic length scale. If this experiment is repeated under almost identical conditions, the generated structure still shows the same characteristic features of snake-like patterns with a characteristic width, but the specific form of the structure is significantly different.

- **Nucleation:** The occurrence of spinodal decomposition in metal alloys depends on the nature of the quench — it has to be a deep quench to a low temperature. On the other hand, shallow quenches leading to slightly higher temperatures can trigger a different instability in the alloy which is called nucleation. In this process, island-like regions, or droplets, which are rich in one of the components form at random positions within the alloy and start to grow. Also in this situation, different experiments result in different sizes and locations of the droplets, regardless of how carefully the initial conditions are chosen.

The occurrence of these instabilities in metal alloys can have profound implications on the properties of the material. Depending on the situation these may be desirable or undesirable. Therefore, information regarding the nature and the time frame of the induced phase separation is of utmost importance. In order to take these — in many situations unavoidable — effects into account, one needs accurate information on the geometry of the patterns, on

how exactly they depend on the initial conditions, and on how the wealth of different patterns can be explained. It is clear from the above descriptions that both phenomena contain some element of stochasticity. How does it enter precisely? What can one expect in a "typical" situation? For example in nucleation, where does the first droplet nucleate most likely?

One of the early models for phase separation phenomena in binary, or two-component, alloys is due to Cahn and Hilliard [12, 13]. They introduced the partial differential equation

$$\partial_t w = -\Delta\left(\varepsilon^2 \Delta w + f(w)\right) \quad \text{in} \quad G\,, \tag{1}$$

subject to homogeneous Neumann boundary conditions for w and Δw. The variable w is an order parameter which describes the local composition of the material. For $w \approx \pm 1$ the material is in either of the two pure phases, values in between indicate a corresponding mixture of the two alloy components. The domain $G \subset \mathbb{R}^d$ is bounded with appropriately smooth boundary, $d \in \{1,2,3\}$, and the function $-f$ is the derivative of a double-well potential F, the standard example being $f(w) = w - w^3$. See also Figures 1 and 2. The small parameter $\varepsilon > 0$ models interaction length. The Cahn-Hilliard equation generates gradient dynamics with respect to the standard van der Waals free energy functional [63]

$$E_\varepsilon[w] = \int_G \left(\frac{\varepsilon^2}{2} \cdot |\nabla w|^2 + F(w) \right) dx\,, \tag{2}$$

which in addition conserves the total mass $\int_G w\,dx$.

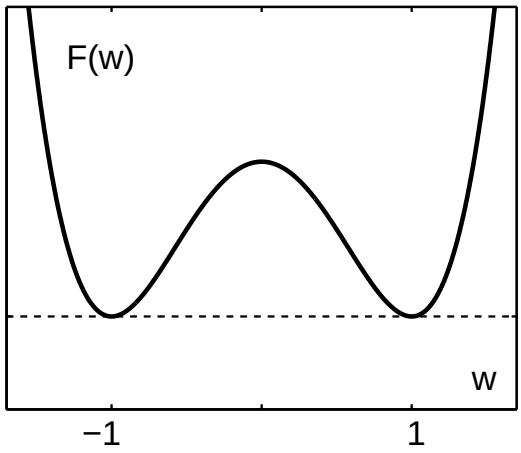

Figure 1: The double-well potential F. The minima at ± 1 correspond to the two alloy components.

For (1), one can give the following heuristic explanation for both spinodal decomposition and nucleation [14, 25]. After quenching, the alloy is more or less homogeneous, i.e., we have $w \approx \bar{w} \equiv m$. The constant function $\bar{w} \equiv m$ is an equilibrium solution of (1), and

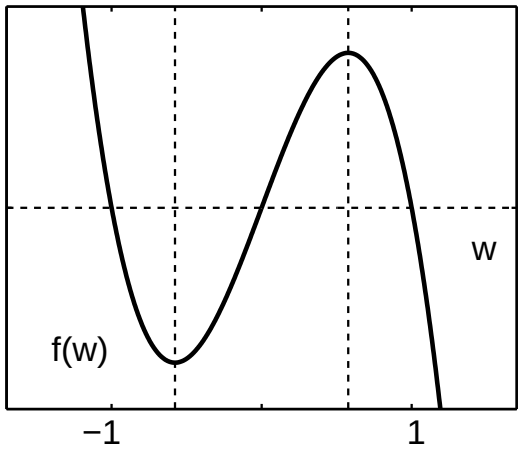

Figure 2: The cubic nonlinearity f. The spinodal region lies between the dashed vertical lines, the metastable region outside.

one can easily verify that its stability for small $\varepsilon > 0$ depends on the sign of the derivative $f'(m)$. For $f'(m) > 0$, the equilibrium $\bar{w}$ is unstable, leading to spontaneous phase separation throughout the alloy, i.e., to spinodal decomposition. On the other hand, for $f'(m) < 0$ the equilibrium $\bar{w}$ is asymptotically stable. While this obviously implies that for small perturbations of $\bar{w}$ the dynamics of (1) drive the system back to the homogeneous state, it is possible that $\bar{w}$ is only a local minimizer of the energy (2). If we perturb the homogeneous equilibrium by a local, yet sufficiently large disturbance, we might push the system into the domain of attraction of the global minimizer of the energy, or at least into the domain of attraction of a state with lower energy. The solution then would converge to this lower energy state, thereby leading to phase separation. This latter process is referred to as nucleation.

The Cahn-Hilliard model has been used successfully for describing phase separation phenomena, see for example the survey by Novick-Cohen [56] and the references therein. Recent mathematical results address both spinodal decomposition [31, 48, 49, 57, 58, 65] and nucleation [3].

Nevertheless, the model (1) is an idealization. It completely ignores thermal fluctuations which are present in any material. In order to address this shortcoming, Cook [17] extended the Cahn-Hilliard equation by incorporating random thermal fluctuations into the model, see also Langer [43]. In the physics literature, the resulting model is called Model B in the classification of Hohenberg and Halperin [36]. The *Cahn-Hilliard-Cook equation* for binary metal alloys is given by

$$\partial_t w = -\Delta\left(\varepsilon^2 \Delta w + f(w)\right) + \sigma_{\text{noise}} \cdot \xi \quad \text{in} \quad G \tag{3}$$

where the additive noise term ξ is usually chosen as space-time white noise or colored noise. In our studies the noise coefficient may depend on ε, i.e. $\sigma_{\text{noise}} = \sigma_\varepsilon$.

We are mainly interested in the evolution of (3) starting at the homogeneous state $w(0) \equiv m$, in order to understand the effects of the additive noise term. Thus, we introduce the change of variables $w = m + u$ and consider the initial value problem

$$\partial_t u = -\Delta\left(\varepsilon^2 \Delta u + f(m+u)\right) + \sigma_{\text{noise}} \cdot \xi \quad \text{in} \quad G\,, \qquad \text{and} \qquad u(0) = 0\,. \tag{4}$$

As in the deterministic case, the stochastic partial differential equation in (4) is complemented by homogeneous Neumann boundary conditions for both u and Δu.

In this survey, we describe recent progress on studying the phase separation dynamics of the initial value problem (4). In particular, we hope to demonstrate that for many aspects of the separation process, the stochastic model is more natural than the deterministic version. Yet, it will become clear that the deterministic model provides an enormous amount of information relevant for the stochastic dynamics. Particular emphasis is put on describing the similarities and the differences between the deterministic and the stochastic model. We show that in order to understand phase separation phenomena in binary alloys, a thorough understanding of both models is necessary.

The paper is organized as follows. In Section 2 we provide a self-contained introduction to stochastic partial differential equations, geared towards our study of the Cahn-Hilliard-Cook model. Section 3 surveys recent mathematical results on spinodal decomposition for solutions of (4) from [9, 10]. In Section 4 we address nucleation in the stochastic model, in particular its relation to the deterministic attractor structure.

2 The Cahn-Hilliard-Cook Model

In this section we provide a self-contained description of the Cahn-Hilliard-Cook model from a dynamical point of view. We present the necessary background on Wiener processes in Hilbert spaces to model the noise term ξ in (3), including a discussion of the correlation functional, the covariance operator, the induced stochastic convolution, and its existence and regularity theory. The existence of solutions to the nonlinear stochastic evolution equation corresponding to (3) is established using the fractional power space setting.

2.1 Wiener Processes in Hilbert Space

Noise processes ξ, such as the one in the Cahn-Hilliard-Cook equation (3), are usually defined as the generalized derivative of some Wiener process in a suitable Hilbert space. As such, they are not stochastic processes in the usual sense, but have to be interpreted in a distributional setting. For classical references we refer the reader to [39] and the references therein.

In order to explain the statements of the last paragraph in more detail, we begin with a definition of generalized stochastic processes. Let $G \subset \mathbb{R}^d$ be a bounded domain with sufficiently smooth boundary, and let $\mathcal{D} = C_0^\infty(\mathbb{R}_0^+ \times G)$ denote the space of smooth functions from $\mathbb{R}_0^+ \times G$ to $\mathbb{R}$ with compact support, where $\mathbb{R}_0^+ = [0,\infty)$. Then the space of *generalized functions* or *distributions* is defined as the dual space $\mathcal{D}^*$ of $\mathcal{D}$, see for example [62].

Furthermore, we define the space $\mathcal{D}_2^*$ consisting of all *bilinear functionals* on $\mathcal{D}$. Finally, $(\Omega, \mathcal{F}, \mathbb{P})$ denotes an abstract probability space. Using this framework, the definition of generalized stochastic process is as follows.

Definition 2.1 *A* generalized stochastic process ξ *is a $\mathcal{D}^*$-valued random variable. In other words, it is given by a measurable function $\xi : \Omega \to \mathcal{D}^*$. Associated with a generalized stochastic process one can consider the* Gaussian system $\{\langle \xi, \varphi \rangle\}_{\varphi \in \mathcal{D}}$*, which is obtained by evaluating ξ at elements $\varphi \in \mathcal{D}$ using the duality $\langle \cdot, \cdot \rangle$ between $\mathcal{D}^*$ and $\mathcal{D}$.*

Finally, we say that the process ξ is a Gaussian process*, if all vector-valued random variables $(\langle \xi, \varphi_1 \rangle, \ldots, \langle \xi, \varphi_n \rangle)$ are Gaussian, for all $n \in \mathbb{N}$ and $\varphi_1, \ldots, \varphi_n \in \mathcal{D}$.*

Just as with standard stochastic processes, the mean value and the correlation functional are important characteristics of a generalized stochastic process. They are defined as follows.

Definition 2.2 *Let ξ denote a generalized Gaussian process. Then its* mean value functional $\mathbb{E}\xi \in \mathcal{D}^*$ *is defined by*

$$\langle \mathbb{E}\xi, \varphi \rangle := \mathbb{E}\langle \xi, \varphi \rangle \quad \textit{for all} \quad \varphi \in \mathcal{D} \, .$$

The correlation functional C_ξ *of ξ is the generalized function in $\mathcal{D}_2^*$ defined by*

$$C_\xi : (\varphi, \psi) \mapsto \mathbb{E}\langle \xi, \varphi \rangle \langle \xi, \psi \rangle \, .$$

In general, the mean value functional $\mathbb{E}\xi$ is not a classical function of t and x, but rather a distribution in $\mathcal{D}^*$. Nevertheless, sufficiently smooth distributions may be represented as functions of t and x. Therefore, we sometimes write $\mathbb{E}\xi = \mathbb{E}\xi(t,x)$, if we want to emphasize the usual physics notation. Similarly, we use $C_\xi = \mathbb{E}\xi(t,x)\xi(s,y)$ for the correlation functional. Notice also that since $\mathbb{E}\langle \xi, \varphi \rangle^2 \geq 0$ for all $\varphi \in \mathcal{D}$, a generalized stochastic process always has a positive semidefinite and symmetric correlation functional.

Constructing generalized Gaussian processes can be accomplished as in the case of classical stochastic processes. Starting from a mean value and correlation functional, the celebrated extension theorem of Kolmogorov ensures the existence of a corresponding Gaussian generalized stochastic process, such that the Gaussian probability measure $\mathbb{P}^\xi$ induced on the space of generalized functions $\mathcal{D}^*$ is uniquely determined.

In our situation we are interested in generalized Gaussian stochastic processes having mean value and correlation functionals of the form

$$\mathbb{E}\xi(t,x) = 0 \, , \qquad \mathbb{E}\xi(t,x)\xi(s,y) = \delta(t-s) \cdot q(x,y) \, , \tag{5}$$

where δ denotes the delta distribution and q is a positive semidefinite and symmetric kernel on $G \times G$. Recall that a kernel is called *symmetric*, if we have $q(x,y) = q(y,x)$ for all $x, y \in G$. Moreover, the kernel q is called *positive semidefinite*, if for all $\varphi \in C_0^\infty(G)$ we have

$$\int_G \int_G q(x,y) \cdot \varphi(x) \cdot \varphi(y) \, dxdy \geq 0 \, .$$

Of particular interest in applications is *homogeneous noise*, for which the kernel q is only a function of the difference $x-y$, i.e., we have $q(x,y) = R(x-y)$ for some function R. In this case, the kernel q is positive semidefinite if and only if R is positive semidefinite, which means that for $x_1,\ldots,x_n \in G$ and $y_1,\ldots,y_n \in \mathbb{R}$ we always have

$$\sum_{j,k=1}^{n} y_j \cdot y_k \cdot R(x_j - x_k) \geq 0 \,.$$

As we mentioned in the beginning of this section, noise processes ξ are generally generated through a differentiation process from Wiener processes in Hilbert space. For this, define the *generalized derivative* $\partial_t \eta$ of a generalized Gaussian stochastic process η in the sense of distributions, i.e., let

$$\langle \partial_t \eta, \varphi \rangle := -\langle \eta, \partial_t \varphi \rangle \quad \text{for all} \quad \varphi \in \mathcal{D} \,.$$

The generalized derivative is again a generalized Gaussian process. One can readily verify that its mean value functional is given by $\partial_t \mathbb{E}\eta(t,x) \in \mathcal{D}^*$, and its correlation functional is given by $\partial_t \partial_s \mathbb{E}\eta(t,x)\eta(s,y) \in \mathcal{D}_2^*$. Generalized derivatives with respect to x, or higher derivatives, can be defined analogously. A well-known example of this situation is the Brownian sheet, which has space-time white noise as its derivative with respect to all variables. For more details we refer the reader to [64, p. 284].

We now leave the discussion of generalized stochastic processes and turn our attention to Wiener processes in Hilbert space. These processes are classical stochastic processes, and their precise definition is as follows.

Definition 2.3 *Let H denote an arbitrary real Hilbert space with inner product $\langle \cdot,\cdot \rangle_H$. Then a* Q-Wiener process *$W = \{W(t)\}_{t\geq 0}$ on H is defined as an H-valued stochastic process $\{W(t)\}_{t\geq 0}$ over $(\Omega, \mathcal{F}, \mathbb{P})$ with the following properties:*

(a) W has continuous paths and satisfies $W(0) = 0$.

(b) W has independent increments, i.e., for all $n \in \mathbb{N}$ and $0 < t_1 < \ldots < t_n$ the random variables $W(t_n) - W(t_{n-1}), \ldots, W(t_2) - W(t_1), W(t_1)$ are independent.

(c) W is a Gaussian process in the sense that $(\langle W(t_1), h_1 \rangle_H, \ldots, \langle W(t_n), h_n \rangle_H)$ is a vector-valued Gaussian random variable for all $n \in \mathbb{N}$, $t_i \geq 0$, and $h_i \in H$.

(d) $\mathbb{E}W(t) = 0$ for all $t \geq 0$, i.e., we have $\mathbb{E}\langle W(t), u \rangle_H = 0$ for all $t \geq 0$ and $u \in H$.

(e) W has a positive semidefinite symmetric covariance operator $Q : H \to H$, i.e., we have $\mathbb{E}\langle W(t), u \rangle_H \langle W(s), v \rangle_H = \min\{t,s\} \cdot \langle Qu, v \rangle_H$ for all $t,s \geq 0$ and $u,v \in H$.

For more details we refer the reader to [20, Section 4], which contains an extensive survey of Q-Wiener processes.

For a given Q-Wiener process we can define a corresponding noise process ξ by considering $\xi = \partial_t W$ in the sense of generalized stochastic processes. However, it is not immediately clear how this differentiation process can generate a noise process ξ satisfying (5) for a given correlation kernel q.

In order to explain this relation, we consider the Hilbert space $H = L^2(G)$ and define the Hilbert-Schmidt operator $Q : L^2(G) \to L^2(G)$ with kernel $q \in L^2(G \times G)$ by

$$(Qf)(x) := \int_G q(x,y) f(y)\, dy \qquad \text{for all} \qquad f \in L^2(G)\,. \tag{6}$$

The following result shows that choosing the function q in the definition of the covariance operator is justified.

Theorem 2.4 [7, Theorem 3.3] *Assume that G is a rectangular or circular domain. Let $q \in L^2(G \times G)$ be a symmetric and positive semidefinite kernel with corresponding Hilbert-Schmidt operator Q on $L^2(G)$ given by (6). Moreover, assume that* $\operatorname{tr}(Q) < \infty$.

Then a Q-Wiener processes W defines a generalized Gaussian process $\xi = \partial_t W$ which satisfies (5). Conversely, if ξ is a generalized Gaussian process satisfying (5), then there exists a Q-Wiener process W such that the generalized derivative $\partial_t W$ is a version of ξ.

The above result shows that there is basically a one-to-one correspondence between generalized Gaussian processes ξ satisfying (5) and Q-Wiener processes with covariance operator as in (6). We would like to point out that results similar to Theorem 2.4 are well-known for homogeneous noise processes on $\mathbb{R}^d$ or on a torus. The novelty of the above result is that it extends these results to the case of non-homogeneous noise processes ξ satisfying (5). Furthermore, we formulated Theorem 2.4 only for special domains, even though the result holds for more general domains satisfying a certain geometric condition. For more details we refer the reader to [7].

2.2 The Linearized Cahn-Hilliard Operator

Before we turn our attention to the linearized Cahn-Hilliard-Cook model, we have to recall some facts about the linearization of the deterministic model (1) at the homogeneous state m.

Definition 2.5 *Consider the linear operator A_ε defined by*

$$A_\varepsilon v := -\Delta\left(\varepsilon^2 \Delta v + f'(m) v\right) \tag{7}$$

on the domain

$$D(A_\varepsilon) = \left\{ v \in X \cap H^4(G) \,:\, \frac{\partial v}{\partial \nu}(x) = \frac{\partial \Delta v}{\partial \nu}(x) = 0\,,\, x \in \partial G \right\}\,,$$

where

$$X = \left\{ v \in L^2(G) \,:\, \int_G v\, dx = 0 \right\}\,.$$

It is well-known that the operator A_ε defined above is self-adjoint. In order to describe its spectrum, let $0 < \mu_1 \leq \mu_2 \leq \ldots \to +\infty$ denote the eigenvalues of the negative Laplacian $-\Delta : X \to X$ subject to homogeneous Neumann boundary conditions, and let $\psi_1, \psi_2, \ldots$ denote the complete $L^2(G)$-orthonormal set of corresponding eigenfunctions. Then the spectrum of A_ε consists of the real eigenvalues

$$\lambda_{k,\varepsilon} = \mu_k \cdot \left(f'(m) - \varepsilon^2 \cdot \mu_k \right) , \quad k \in \mathbb{N} , \tag{8}$$

and the eigenfunction associated with $\lambda_{k,\varepsilon}$ is given by ψ_k, for $k \in \mathbb{N}$.

For our applications it is essential to have precise knowledge of the asymptotic behavior of the eigenvalues μ_k. For the case of domains G with piece-wise C^1-boundary this behavior is well-known. According to [18, p. 442] or [23] we have

$$\lim_{k\to\infty} \mu_k \cdot k^{-2/\dim G} = C_G > 0 , \tag{9}$$

where the positive constant C_G depends only on the domain G. In order to describe the spectrum further, we introduce

$$\lambda_\varepsilon^{\max} := \sup \left\{ \mu \left(f'(m) - \varepsilon^2 \mu \right) \, : \, \mu > 0 \right\} = \begin{cases} \dfrac{f'(m)^2}{4\varepsilon^2} & \text{for} \quad f'(m) > 0 , \\ 0 & \text{for} \quad f'(m) \leq 0 . \end{cases} \tag{10}$$

Using the operator A_ε we can now introduce the Hilbert space that serves as phase space for the nonlinear evolution equation (3). For this, recall that the operator $-A_\varepsilon$ is sectorial, i.e., we can use it to define fractional power spaces as in [35]. More precisely, for $C_\varepsilon = c \cdot \lambda_\varepsilon^{\max}$, where $c > 1$, and arbitrary $0 \leq s \leq 1$ we define the space

$$X^s := D\left((C_\varepsilon - A_\varepsilon)^s\right) \quad \text{equipped with the norm} \quad \|\cdot\|_s = \left\| \Delta^{2s} \cdot \right\|_{L^2(G)} .$$

We would like to point out that the norm $\|\cdot\|_s$ is not the canonical graph norm on X^s, but rather an equivalent one which is more appropriate for our applications.

In the following we will use the space $X^{1/2}$, which turns out to be a subspace of the Sobolev space $H^2(G)$. Even though this is not immediately clear from its definition, the space $X^{1/2}$ is in fact independent of ε, see for example [49, Lemma 3.2] and [61, Lemma III.4.2]. We equip $X^{1/2}$ with the norm $\|\cdot\|_* = \|\cdot\|_{1/2}$, which is equivalent to the standard $H^2(G)$-norm. One of the main advantages of using the norm $\|\cdot\|_*$ on $X^{1/2}$ is that it is ε-independent as well and can easily be written as a weighted ℓ^2-norm in Fourier space, i.e., we have

$$\left\| \sum_{k=1}^{\infty} \gamma_k \cdot \psi_k \right\|_* = \left(\sum_{k=1}^{\infty} \mu_k^2 \cdot \gamma_k^2 \right)^{1/2} \qquad \text{for all} \qquad \sum_{k=1}^{\infty} \gamma_k \cdot \psi_k \in X^{1/2} .$$

In fact, it was shown in [49] that a function $u = \sum_{k=1}^{\infty} \gamma_k \psi_k$ is contained in the fractional power space $X^{1/2}$ if and only if $\sum_{k=1}^{\infty} \mu_k^2 \gamma_k^2 < \infty$.

2.3 The Stochastic Convolution

Next we turn our attention to the linearized Cahn-Hilliard-Cook model, since it will be the key for obtaining existence and regularity results for the nonlinear model. Linearizing (3) at the homogeneous state m we obtain the linear stochastic evolution equation

$$\partial_t v = A_\varepsilon v + \sigma_\varepsilon \cdot \partial_t W \ , \tag{11}$$

where A_ε was defined in Definition 2.5, and W in Definition 2.3. We assume that the range of the covariance operator Q is orthogonal to the constant functions, which guarantees that the linear equation (11) is mass conserving.

As in the deterministic case, it is possible to represent the solution of (11) explicitly. To this end, define the *stochastic convolution* as

$$W_{A_\varepsilon}(t) = \int_0^t e^{(t-\tau)A_\varepsilon}\, dW(\tau) \ , \tag{12}$$

where e^{tA_ε} denotes the analytic semigroup generated by A_ε. Then for given noise strength σ_ε, the process $\sigma_\varepsilon \cdot W_{A_\varepsilon}$ solves (11) subject to the initial condition $v(0) = 0$. We would like to point out that the integral in (12) is not a classical Riemann-Stieltjes integral, but rather a stochastic integral. For more details on stochastic integration, we refer the reader to [20]. The stochastic convolution is fundamental for the study of stochastic evolution equations and a detailed discussion of its properties can be found in [20, Section 5]. Of particular interest for our study are the regularity properties of W_{A_ε}, since they will be used to establish the existence and regularity of solutions of the nonlinear Cahn-Hilliard-Cook model (3).

In order to guarantee that the stochastic convolution W_{A_ε} is a continuous Gaussian process in certain fractional power spaces X^s, we need to introduce conditions on the covariance operator Q of W. More precisely, the stochastic convolution has a version in the space $C([0,T],X^s)$, provided we have

$$\operatorname{tr}\left(\int_0^T \tau^{-\alpha}\Delta^{2s} e^{\tau A_\varepsilon} Q e^{\tau A_\varepsilon}\Delta^{2s}\, d\tau\right) < \infty \ , \tag{13}$$

for some $\alpha > 0$. For the case $s = 0$ this result was established in [20, Section 5.3], the case $s = 1$ can be found in [19, Proposition 1.2]. The general case can be obtained in a similar way.

The condition in (13) relates the covariance operator to both the Laplacian and the linearized Cahn-Hilliard operator. All of these operators are symmetric, and it was shown in Section 2.2 that the latter two have a joint complete set of eigenfunctions. It would simplify matters greatly, if also Q had the same set of eigenfunctions — but for which correlation kernels q can this be achieved? One can easily show that Q and the Laplacian Δ have the same set of eigenfunctions if and only if Q and Δ commute. This latter property can be related to the correlation kernel q in (6).

Theorem 2.6 [7, Theorem 4.2] *Consider a symmetric and positive semidefinite function $q \in L^2(G \times G)$, and let the corresponding operator Q on $L^2(G)$ be defined as in (6). Then Q commutes with Δ if and only if*

$$\int_G \int_G q(x,y) \cdot (\Delta_y - \Delta_x) \cdot \varphi(x)\psi(y)\, dxdy = 0 \quad \textit{for all} \quad \varphi, \psi \in D(\Delta)\,. \tag{14}$$

Theorem 2.6 holds for a variety of boundary conditions associated with Δ, in particular for homogeneous Dirichlet or Neumann boundary conditions, as well as periodic boundary conditions. For more detail we refer the reader to [7]. The condition (14) can easily be recognized as the weak formulation of a suitable partial differential equation for q. For simple domains, such as rectangular domains, this partial differential equation can be solved, and hence be used to characterize correlation kernels q which imply that Q and Δ commute. For the case of an interval and homogeneous Neumann boundary conditions, one obtains the following result.

Corollary 2.7 [7, Theorem 4.8] *Let $G = (0,L)$ be an interval, and consider a symmetric, positive semidefinite, and sufficiently smooth kernel q, say $q \in C^2(G \times G)$. Moreover, consider the operator Q defined in (6). Then Q commutes with Δ subject to homogeneous Neumann boundary conditions if and only if there exists a $2L$-periodic even function R such that $q(x,y) = R(x-y) + R(x+y)$.*

The correlation kernels q in the above corollary are not homogeneous, see Figure 3 for a typical example. In fact, if the correlation kernel q is homogeneous and nonzero, then the covariance operator Q never commutes with the Laplacian subject to homogeneous Neumann boundary conditions [7, Corollary 4.9].

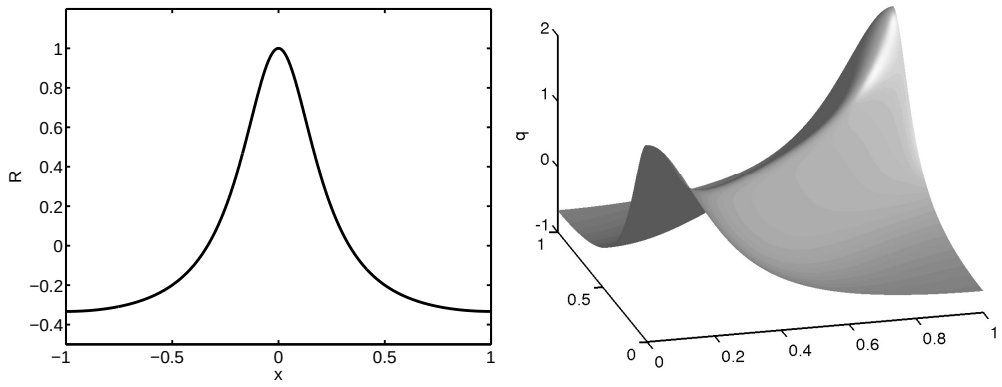

Figure 3: A positive semidefinite correlation kernel $q(x,y) = R(x-y) + R(x+y)$, whose covariance operator Q commutes with the Laplacian subject to Neumann boundary conditions.

Despite the restrictiveness of the assumption that Q commutes with the Laplacian, it is widely used — and we will make no exception. This assumption allows us to expand the

stochastic convolution in a Fourier series with respect to the eigenfunctions of the Laplacian Δ. Moreover, since Q also commutes with the linearized Cahn-Hilliard operator A_ε, we can study the dynamics of the stochastic convolution restricted to subspaces spanned by the eigenfunctions of A_ε.

Thus, in the following we assume that Q commutes with Δ, and hence also with A_ε, and that the range of Q is orthogonal to the constant functions. In this situation, the three operators Q, Δ, and A_ε have a joint set of eigenfunctions in $X \subset L^2(G)$, and [20, Proposition 4.1] shows that a Q-Wiener process W can be written as a Fourier series of the form

$$W(t) = \sum_{k=1}^{\infty} a_k \cdot \beta_k(t) \cdot \psi_k \,. \tag{15}$$

In this representation, $\{\beta_k\}_{k\in\mathbb{N}}$ denotes a family of independent real-valued standard Brownian motions, the functions ψ_k are the eigenfunctions of the Laplacian subject to homogeneous Neumann boundary conditions, and $Q\psi_k = a_k^2 \cdot \psi_k$. Using the representation (15) in combination with (12), we further obtain

$$W_{A_\varepsilon}(t) = \sum_{k=1}^{\infty} a_k \cdot \int_0^t e^{(t-\tau)\lambda_{k,\varepsilon}}\, d\beta_k(\tau) \cdot \psi_k \,, \tag{16}$$

where the integrals are real stochastic integrals.

We now return to our study of the regularity properties of the stochastic convolution, and hence to the condition given in (13). Its validity crucially depends on the asymptotic behavior of the coefficients a_k in (15) or (16), in particular relative to the eigenvalues μ_k of the negative Laplacian. For simplicity, we assume that there exists a regularity constant $s_* > 0$ such that

$$a_k^2 \cdot \mu_k^{s_*} \to C \qquad \text{for} \qquad k \to \infty \,.$$

Then one can easily show that (13) is satisfied as long as $s_* + 2 - 4s > d/2$, i.e., we have

$$W_{A_\varepsilon} \in C\left([0,T], X^s\right) \qquad \text{if and only if} \qquad s_* > 4s - 2 + \frac{d}{2} \,, \tag{17}$$

where $d = \dim G$. This regularity result will suffice to study existence and regularity questions for the nonlinear Cahn-Hilliard-Cook equation in Section 2.4. Moreover, it can be used to establish spatial regularity of the stochastic convolution in the spaces $C^\ell(G)$ for $\ell \geq 0$. One can easily show that the fractional power space X^s is continuously embedded in the Sobolev space $H^{4s}(G)$. If we then combine (17) with Sobolev's embedding theorem [1], one can see that

$$W_{A_\varepsilon} \in C\left([0,T], C^\ell(G)\right) \,, \qquad \text{as long as} \qquad s_* > \ell - 2 + d \,.$$

We would like to point out, however, that this last inequality is not a necessary condition. By imposing fairly restrictive conditions on the base domain G one can show that in fact

$$W_{A_\varepsilon} \in C\left([0,T], C^\ell(G)\right) \,, \qquad \text{as long as} \qquad s_* > \ell - 2 + \frac{d}{2} \,. \tag{18}$$

This result can be proved using Kolmogorov's test. For $\ell = 0$ we refer the reader to [20, Theorem 5.20], the case $\ell > 0$ can be found in [6, Section 2.2.2]. We will encounter the precise definition of the necessary conditions on the domain G later in Assumption 3.1. These conditions are satisfied for example for rectangular domains in one, two, and three space dimensions, but they are not satisfied for discs in two dimensions.

Before addressing existence and regularity results for the nonlinear Cahn-Hilliard-Cook model, we summarize our assumptions on the noise process.

Assumption 2.8 *Let W be a Q-Wiener process with covariance operator Q as in (6), and consider the associated generalized Gaussian noise process $\xi = \partial_t W$ satisfying (5). In addition, assume that the symmetric and positive semidefinite correlation kernel q satisfies*

$$\int_G q(x,y)\,dx = 0 \qquad \text{for all} \qquad y \in G\,,$$

and that q implies the commutativity of Q and the Laplacian subject to homogeneous Neumann boundary conditions (via (14)). Finally, assume that the coefficients a_k in the resulting Fourier series expansion (15) satisfy

$$\lim_{k\to\infty} a_k^2 \cdot \mu_k^{s_*} = C\,, \qquad \text{where} \qquad s_* > \frac{d}{2}\,.$$

Notice that in terms of regularity, the above assumption corresponds to $s = 1/2$ in (17). In other words, Assumption 2.8 implies that the stochastic convolution W_{A_ε} has a version in the space $C([0,T], X^{1/2})$. As we mentioned above, the space $X^{1/2}$ is continuously embedded in the Sobolev space $H^2(G)$.

In the situation of Assumption 2.8, one can easily derive an explicit representation for the correlation kernel q. If $\{\psi_k\}_{k\in\mathbb{N}}$ denotes the system of $L^2(G)$-orthonormalized eigenfunctions of $-\Delta$ on X subject to homogeneous Neumann boundary conditions, then

$$q(x,y) = \sum_{k=1}^{\infty} a_k^2 \cdot \psi_k(x) \cdot \psi_k(y) \qquad \text{for all} \qquad x,y \in G\,.$$

It is a consequence of Mercer's theorem [18, Section 3.5.4] that for continuous q this series converges uniformly on $G \times G$. The correlation kernel q in Figure 3 corresponds to the choice $a_k^2 = 1/2^k$ for $k \in \mathbb{N}$.

Let us close with a comment on the considered noise processes ξ. In order to keep our presentation as accessible as possible, we considered only the case of a sufficiently smooth correlation kernel q and assumed that the covariance operator Q has a finite trace $\operatorname{tr} Q$. In fact, notice that the condition $\operatorname{tr} Q < \infty$ is equivalent to obtaining an $H^2(G)$-valued stochastic convolution W_{A_ε}. This condition can of course be relaxed. It is possible to consider cylindrical Wiener processes W which do not converge in $L^2(G)$, but in larger spaces of distributions. In this case, the smoothing effect of the analytic semigroup generated by A_ε still increases the regularity, and it is possible to obtain the expansion (16). In this way, space-time white noise can be treated. For more details we refer the reader to [6, 9, 20].

2.4 Existence and Regularity Results

We finally turn our attention to the nonlinear Cahn-Hilliard-Cook equation. Rather than studying its original form (3), we concentrate on the transformed equation (4) from now on. Formally, this equation can be rewritten as the abstract nonlinear stochastic evolution equation

$$\partial_t u = A_\varepsilon u + F(u) + \sigma_\varepsilon \cdot \partial_t W \ , \tag{19}$$

where the nonlinearity F is given by

$$F(u) := -\Delta g(u) \qquad \text{and} \qquad g(u) := f(m+u) - f'(m)u - f(m) \ . \tag{20}$$

In order to define a suitable solution concept for (19) we formally integrate the equation. Thus, a stochastic process u is called mild solution of (19), if it satisfies the variation of constants formula

$$u(t) = e^{tA_\varepsilon}u(0) + \int_0^t e^{(t-\tau)A_\varepsilon}F(u(\tau))\,d\tau + \sigma_\varepsilon \cdot W_{A_\varepsilon}(t) \ , \tag{21}$$

where W_{A_ε} denotes the stochastic convolution defined in (12).

Under suitable conditions on the nonlinearity f, the global existence of a unique mild solution of the Cahn-Hilliard-Cook equation (19) has been established in [19]. However, for the situation considered in this paper we only need the existence of a local mild solution in the fractional power space $X^{1/2}$. For this, we need the following assumption on the nonlinearity g.

Assumption 2.9 *Let g and F be as in (20), and assume that $g : \mathbb{R} \to \mathbb{R}$ is smooth and at least quadratic for small u. More precisely, suppose that $g(u) = u^{1+\kappa} \cdot \tilde{g}(u)$, where $\kappa \geq 1$ and $\tilde{g}$ is a C^2-function on an interval containing 0.*

Under this assumption, one can easily show that the nonlinearity F is a differentiable operator from $X^{1/2}$ to X with $F(0) = 0$ and $DF(0) = 0$, see for example [31, Section 4.1]. If we further assume that the stochastic convolution W_{A_ε} is sufficiently regular, then one can employ standard fixed point arguments as in [35, Section 3.3] to solve (21) pathwise. This leads to the following result.

Proposition 2.10 *Suppose that Assumptions 2.8 and 2.9 are satisfied, and assume that $u(0) \in X^{1/2}$ almost surely. Then the Cahn-Hilliard-Cook equation (19) has a unique local mild solution u originating at $u(0)$. In other words, u is a stochastic process satisfying $u \in C([0,T^*), X^{1/2})$ for some positive stopping time T^*, which satisfies (21) for all $t \in [0,T^*)$. In addition, we either have $T^* = \infty$ or $\|u(T^*)\|_* = \infty$.*

The main reason for working in the fractional power space $X^{1/2} \subset H^2(G)$ is that we want to control the $L^\infty(G)$-norm of the solution in three space dimensions. Otherwise, we could easily use spaces of less regularity allowing for less regular noise. Notice also that the specific local growth of g near the origin is not necessary for obtaining Proposition 2.10. Yet, this local growth is crucial for our subsequent considerations.

3 Spinodal Decomposition

As we mentioned in the beginning of this survey, the two major phase separation phenomena described by the Cahn-Hilliard models are spinodal decomposition and nucleation — and this section is devoted to the study of the former. For the deterministic Cahn-Hilliard equation spinodal decomposition has been studied extensively in recent years [31, 48, 49, 57, 58, 65]. In this section we survey recent results for the stochastic model [9, 10].

3.1 Assumptions and Basic Framework

In the deterministic situation, spinodal decomposition is a consequence of the instability of the homogeneous equilibrium $\overline{w} \equiv m$ of (1) for $f'(m) > 0$. Most solutions originating in a small neighborhood of the homogeneous state are driven away, thereby exhibiting phase separation.

In the stochastic model, the homogeneous state is no longer an equilibrium solution due to the additive noise term. Thus, in order to understand spinodal decomposition in (3), it suffices to describe the dynamics of the solution originating exactly at the homogeneous state. In other words, our goal is to understand the behavior of "generic" solution paths of the transformed initial value problem (4). Following the notation of the last section, we consider the mild solution u of the abstract initial value problem

$$\partial_t u = A_\varepsilon u + F(u) + \sigma_\varepsilon \cdot \partial_t W \qquad \text{with} \qquad u(0) = 0\,, \tag{22}$$

where A_ε was defined in (7) and F in (20). Recall that $F(0) = 0$ and $DF(0) = 0$. For the remainder of Section 3, we will always assume that Assumptions 2.8 and 2.9 are satisfied, and that $f'(m) > 0$. The results presented in this section also require the following assumption on the domain G.

Assumption 3.1 *Let $G \subset \mathbb{R}^d$, where $d \in \{1,2,3\}$, be a bounded domain with piece-wise C^1-boundary. Furthermore, assume there exist positive constants C_1 and C_2 such that for all $k \in \mathbb{N}$ we have*

$$\|\psi_k\|_{L^\infty(G)} \le C_1 \qquad \textit{and} \qquad \|\nabla \psi_k\|_{L^\infty(G)} \le C_2 \cdot \sqrt{\mu_k}\,, \tag{23}$$

where μ_k and ψ_k denote the eigenvalues and $L^2(G)$-orthonormalized eigenfunctions of the negative Laplacian on X subject to homogeneous Neumann boundary conditions as in Section 2.2.

While this assumption is satisfied for one-dimensional domains, it is fairly restrictive in two and three space dimensions. It can easily be verified for rectangular, hexagonal, or triangular domains, but general conditions on the geometry of G which would imply (23) are not known. Nevertheless, these assumptions are frequently used, and for example crucial to establish regularity of W_{A_ε} in spaces of continuous functions. See [20, p. 139] and the discussion of (18).

Let us return to the dynamics of the mild solution u of (22). Initially, one expects that the dynamics of u is determined by the linearization of the Cahn-Hilliard-Cook equation, which is given by (11). Thus, the spectrum of A_ε, in particular its unstable part, plays a dominant role. Using (8) and (9) one can easily show that the number of positive eigenvalues of A_ε is proportional to $\varepsilon^{-\dim G}$ as $\varepsilon \to 0$. Not all of these eigenvalues are equally important for the initial dynamical behavior. Only the largest ones corresponding to the strongest unstable directions should play a significant role. Isolating these strongly unstable directions leads to the following splitting of our phase space $X^{1/2}$ — which will be fundamental for our study.

Definition 3.2 *Consider two constants $0 < \gamma < \gamma^+ < 1$, which will be specified in more detail later, and define two complementary subspaces of $X^{1/2}$ by*

$$X_\varepsilon^+ = \mathit{span}\,\{\psi_k : \lambda_{k,\varepsilon} \geq \gamma \cdot \lambda_\varepsilon^{\max}\} \quad \textit{and} \quad X_\varepsilon^- = \mathit{span}\,\{\psi_k : \lambda_{k,\varepsilon} < \gamma \cdot \lambda_\varepsilon^{\max}\}\ .$$

We denote the index sets corresponding to X_ε^+ and X_ε^- by Λ_ε^+ and Λ_ε^-, respectively. The $L^2(G)$-orthogonal projections of an element $v \in X^{1/2}$ onto X_ε^+ and X_ε^- are denoted by v^+ and v^-. In addition, consider the subspace $X_\varepsilon^{++} \subset X_\varepsilon^+$ defined by

$$X_\varepsilon^{++} = \mathit{span}\left\{\psi_k : \lambda_{k,\varepsilon} \geq \gamma^+ \cdot \lambda_\varepsilon^{\max}\right\}\ ,$$

and denote the corresponding index set by $\Lambda_\varepsilon^{++} \subset \Lambda_\varepsilon^+$.

The space X_ε^+ consists of all unstable eigendirections which are important for the initial dynamics of u. Thus, it was called *dominating subspace* in [48]. Even though this space corresponds normally only to a small percentage of the unstable eigenvalues, its dimension remains proportional to $\varepsilon^{-\dim G}$ as $\varepsilon \to 0$. The subspace X_ε^{++} has to be introduced for technical reasons, which will be addressed later.

Our description of spinodal decomposition will be given in two stages, each of which corresponds to a certain region in the phase space $X^{1/2} \subset H^2(G)$. Recalling that $X^{1/2}$ was equipped with the norm $\|\cdot\|_* = \|\cdot\|_{1/2}$ in Section 2.3, these regions can be defined as follows.

Definition 3.3 *For given positive constants δ, R, q_0, and r_0, we define the following three subsets of $X^{1/2}$:*

$$\begin{aligned}
\mathcal{C}_\delta &:= \left\{v \in X^{1/2} : \left\|v^-\right\|_* \leq \delta \left\|v^+\right\|_*\right\}\ , \\
\mathcal{K}_{\delta,R} &:= \left\{v \in X^{1/2} : \|v\|_* \leq R \quad \textit{and} \quad v \in \mathcal{C}_\delta\right\}\ , \\
\mathcal{Z}_{q_0,r_0} &:= \left\{v \in X^{1/2} : \left\|v^+\right\|_* \leq r_0 \quad \textit{and} \quad \left\|v^-\right\|_* \leq q_0\right\}\ .
\end{aligned}$$

We would like to point out that since the splitting $X = X_\varepsilon^+ \oplus X_\varepsilon^-$ is ε-dependent, the same applies to the cone $\mathcal{C}_\delta$, the truncated cone $\mathcal{K}_{\delta,R}$, and the cylinder-shaped region $\mathcal{Z}_{q_0,r_0}$. However, we will not mention this dependence explicitly.

Using the above-defined sets, we can give an intuitive description of the dynamics of spinodal decomposition for (22). As we mentioned before, initially we expect the solution

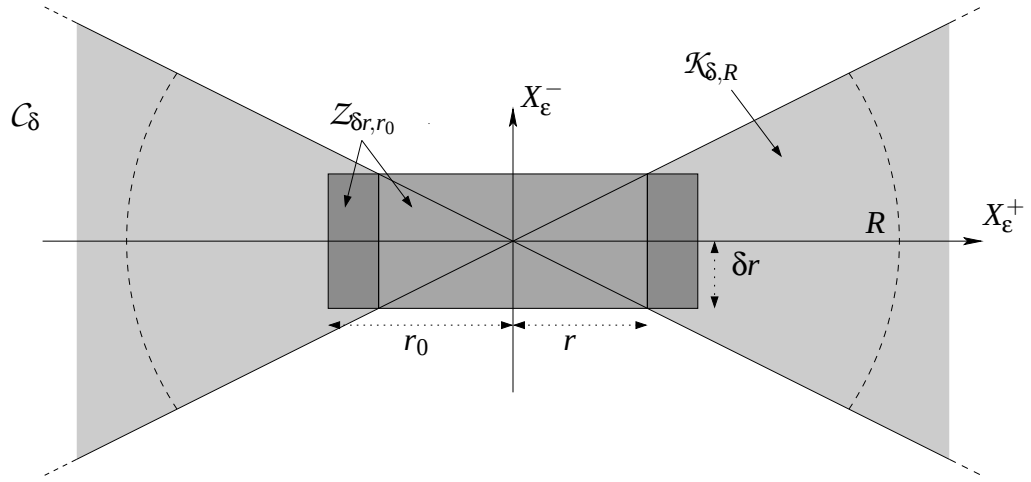

Figure 4: The sets $\mathcal{Z}_{\delta r,r_0}$, $\mathcal{K}_{\delta,R}$, and $\mathcal{C}_\delta$. See Figure 1 of [10].

paths of u to exhibit linearized behavior. Thus, the X_ε^+-component of u should grow considerably faster than the X_ε^--component. This implies that solution paths of (22) are likely to reach the dark shaded regions of $\mathcal{Z}_{\delta r,r_0}$ in Figure 4, at some time t_0. Moreover, we would expect to be able to choose this cylinder fairly narrow, with $\delta r \ll r_0$. In fact, the *first stage of spinodal decomposition* presented in Section 3.2 shows that there exists some deterministic time $t_0 > 0$ such that the subset of Ω defined by

$$\mathcal{N}_1 := \left\{ u(t) \in \mathcal{Z}_{\delta r,r_0} \quad \text{for all} \quad t \in [0,t_0] \,, \quad \left\| u^+(t_0) \right\|_* \geq r \right\}$$

has probability close to one. At the end of the first decomposition stage, the X_ε^+-component of u is considerably larger than the X_ε^--component. Due to [48, Section 4], this implies that the patterns of the functions $u(t_0)$ already exhibit the complicated geometry which is characteristic for spinodal decomposition.

The result on the first stage is a consequence of the smallness of the nonlinearity F on a neighborhood of the initial state 0. In fact, the radius r_0 is a measure for how close one has to stay to 0, before the nonlinearity gets too large. One would therefore expect that after the first stage, nonlinear effects dominate the dynamics of (22) — but this is not the case. In Section 3.3 we will see that for sufficiently small δ, the nonlinearity F remains small on the cone $\mathcal{C}_\delta$ up to a large distance R, even though this is not true outside the cone. Consequently, we find that solution paths of (22) are likely to stay close to X_ε^+ much further. If $T_c > 0$ denotes the exit time of $u(t_0 + \cdot)$ from the cone $\mathcal{K}_{\delta,R}$, then it will be shown in Section 3.3 that the event

$$\mathcal{N}_2 := \left\{ u(t+t_0) \in \mathcal{K}_{\delta,R} \quad \text{for all} \quad t \in [0,T_c] \,, \quad \left\| u(t_0+T_c) \right\|_* = R \right\}$$

still has probability close to one. Since δ is small, this guarantees that the solution u remains close to X_ε^+ until it reaches norm R, and therefore it exhibits the spinodal decomposition

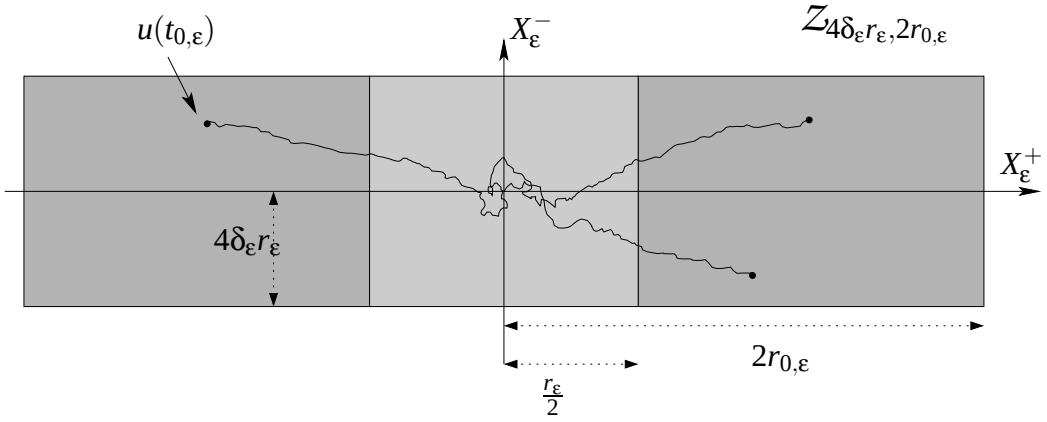

Figure 5: A sketch of three typical trajectories of u during the first decomposition stage. Solution paths exhibiting this behavior correspond to the event $\mathcal{N}_{1,\varepsilon}$.

patterns of functions in the dominating subspace. In fact, we will show that the dynamics of u is driven by the linearized equation (11) throughout $\mathcal{K}_{\delta,R}$. This phenomenon is called *second phase spinodal decomposition.*

Before presenting the results on the two decomposition stages in more detail, let us mention again that (22) is a family of problems depending on the small parameter ε. Therefore, in addition to the splitting $X^{1/2} = X_\varepsilon^+ \oplus X_\varepsilon^-$, all the parameters mentioned above will depend on ε as well, such as δ and $r < r_0 < R$. Moreover, the geometric parameters in the above definitions of the sets $\mathcal{N}_1$ and $\mathcal{N}_2$ will have to be slightly rescaled for the actual nonlinear results. Their definition in this subsection was based on our desire to provide an intuitive description of the decomposition process.

3.2 First Decomposition Stage

We begin by describing the first decomposition stage in more detail. During this stage, solution paths of (22) remain in a cylinder-shaped region which is centered at the origin, small in the X_ε^--direction, but large in the direction of the dominant subspace X_ε^+; see Figure 5. The stage covers a time horizon from $t = 0$, at which the solution starts at the origin, up to a deterministic time $t = t_{0,\varepsilon}$, at which the X_ε^+-component of u is large with high probability. More precisely, at the end of the first decomposition stage, solution paths will be contained in the dark shaded regions of Figure 5.

It is one of the consequences of the stochasticity in the Cahn-Hilliard-Cook model that one is able to obtain a definite deterministic time $t_{0,\varepsilon}$ at which the first decomposition stage is complete and the complicated solution patterns have started to develop. Since the precise definition of $t_{0,\varepsilon}$ is fairly involved [10], we restrict ourselves to describing its asymptotic behavior as $\varepsilon \to 0$. For this, the following assumption and definition prove to be useful.

Assumption 3.4 *Let s_* denote the regularity exponent from Assumption 2.8, and let d denote the dimension of the domain G. Then we define*

$$D := 2s_* - d - 2 \,,$$

and assume further that

$$\Theta_\varepsilon := \frac{r_\varepsilon^2}{\sigma_\varepsilon^2 \cdot \varepsilon^D} \to \infty \qquad \textit{for} \qquad \varepsilon \to 0 \,. \tag{24}$$

Notice that due to Assumption 2.8 we have $D > -2$.

Definition 3.5 *Let f_ε and g_ε denote two real quantities depending on the small parameter $\varepsilon > 0$. Then we say that g_ε* is of order *f_ε, provided there are (ε-independent) positive constants c and C such that $c \cdot f_\varepsilon \le g_\varepsilon \le C \cdot f_\varepsilon$ for all sufficiently small $\varepsilon > 0$. In this case we write $g_\varepsilon = O(f_\varepsilon)$. If on the other hand we have $g_\varepsilon / f_\varepsilon \to 0$ for $\varepsilon \to 0$, then we write $g_\varepsilon = o(f_\varepsilon)$. Finally, we write $g_\varepsilon \in \mathcal{P}_\varepsilon$ if and only if there are positive constants c and C such that $|g_\varepsilon| \le C \cdot \varepsilon^c$ for all sufficiently small $\varepsilon > 0$.*

The quantity Θ_ε introduced in Assumption 3.4 relates the noise strength σ_ε to r_ε, the latter of which is one of the defining parameters of the cylindrical region in Figure 5. In addition, Θ_ε plays an inportant role in describing the asymptotics of the main parameters involved in quantifying the decomposition process.

One of these main parameters is certainly the end time $t_{0,\varepsilon}$ of the first decomposition stage. According to [10], it is of the form

$$t_{0,\varepsilon} = \frac{1}{2\gamma^+ \lambda_\varepsilon^{\max}} \cdot \ln O(\Theta_\varepsilon) \,, \tag{25}$$

where γ^+ was introduced in Definition 3.2, and $\lambda_\varepsilon^{\max}$ was defined in (10). We will see in Section 3.3 that Θ_ε normally is of the order $O(\varepsilon^{\varphi_\Theta})$ for some $\varphi_\Theta < 0$. Thus, the first decomposition stage — which is responsible for the initial pattern selection and formation — takes only a very small amount of time, which is of the order $\varepsilon^2 \cdot \ln(1/\varepsilon)$.

The quantity Θ_ε also determines the relative size of the parameters r_ε and $r_{0,\varepsilon}$. According to [10], they satisfy

$$r_{0,\varepsilon} = r_\varepsilon \cdot O\left(\Theta_\varepsilon^{(1-\gamma^+)/(2\gamma^+)}\right) \,. \tag{26}$$

As is shown in Figure 5, the parameters $r_\varepsilon < r_{0,\varepsilon}$ determine the possible range for the size of the X_ε^+-component of the solution u at the end of the first stage.

The following result is the main theorem on the first decomposition stage. The presented version is taken from [10, Corollary 4.10] and provides a precise estimate on the probability of the random event

$$\mathcal{N}_{1,\varepsilon} := \left\{ u(t) \in \mathcal{Z}_{4\delta_\varepsilon r_\varepsilon, 2r_{0,\varepsilon}} \quad \text{for all} \quad t \in [0, t_{0,\varepsilon}] \,, \quad \left\| u^+(t_{0,\varepsilon}) \right\|_* \ge \frac{r_\varepsilon}{2} \right\} \,. \tag{27}$$

This event corresponds to all solution trajectories exhibiting the dynamics of the first decomposition stage.

Theorem 3.6 *Suppose that Assumptions 2.8, 2.9, 3.1, and 3.4 are satisfied, and assume that $f'(m) > 0$. Consider the operators and spaces introduced in Definitions 2.5 and 3.2. Furthermore, let u denote the mild solution of the stochastic initial value problem (22), and define*

$$\delta_\varepsilon := \delta_0 \cdot \varepsilon^{2-d/2} \qquad \text{for some} \qquad \delta_0 > 0\,. \tag{28}$$

Consider a suitably chosen time $t_{0,\varepsilon}$ satisfying (25), and parameters $r_\varepsilon < r_{0,\varepsilon}$ satisfying (24), (26), as well as $r_{0,\varepsilon} \cdot \delta_\varepsilon = o(1)$. Finally, suppose that $-2 < D < 2$, and that for small positive constants ζ_1 and ζ_2 we have

(S1) $\delta_\varepsilon^{-2} \cdot \Theta_\varepsilon^{-1+\tilde\gamma/\gamma^+} \in \mathcal{P}_\varepsilon$, *where* $\tilde\gamma := \gamma \cdot (1+\zeta_1) < \gamma^+$, *and*

(S2) $\lim\limits_{\varepsilon\to 0} r_\varepsilon^\kappa \cdot \delta_\varepsilon^{\kappa-1} \cdot \Theta_\varepsilon^{\tilde\kappa+1/2} = 0$, *where* $\tilde\kappa := (\zeta_2 + (\kappa+2)\cdot(1-\gamma^+))/(2\gamma^+) > 0$.

Then for any $q > 0$ there exists a constant $C_q > 0$ such that

$$\mathbb{P}\left(\mathcal{N}_{1,\varepsilon}^c\right) \le C_q \cdot \varepsilon^q$$

for all sufficiently small $\varepsilon > 0$, where $\mathcal{N}_{1,\varepsilon}$ was defined in (27). In other words, the probability that a solution path of (22) exhibits the first stage of spinodal decomposition converges to 1 faster than any polynomial in ε.

Proof outline: The proof of the above result splits naturally into two parts. The first part consists of introducing a stochastic event $\Omega_{1,\varepsilon}$ which is defined similar to $\mathcal{N}_{1,\varepsilon}$, but for the solution $\sigma_\varepsilon \cdot W_{A_\varepsilon}$ of the linearized Cahn-Hilliard-Cook equation (11) instead of u. Using the smallness of the nonlinearity F in a small neighborhood of the origin, one can then estimate the difference between the solutions $u(t)$ and $\sigma_\varepsilon \cdot W_{A_\varepsilon}(t)$. This implies that the nonlinear solution paths corresponding to the event $\Omega_{1,\varepsilon}$ exhibit dynamical behavior analogous to the trajectories of the solution to the linearized equation — and by suitably defining $\Omega_{1,\varepsilon}$ this establishes the inclusion $\Omega_{1,\varepsilon} \subset \mathcal{N}_{1,\varepsilon}$. In the second part of the proof, one has to obtain a lower bound on the probability of the event $\Omega_{1,\varepsilon}$. Notice that this event is defined completely in terms of the stochastic convolution W_{A_ε}. Thus, the probability estimates can be obtained by careful estimates of large deviations type. For more details on the proof of Theorem 3.6 we refer the reader to [10]. ◇

The conditions of Theorem 3.6, in particular (S1) and (S2), are fairly elaborate, and it is far from clear whether the involved constants can be chosen appropriately. This question will be answered in the affirmative in Section 3.3. A slightly weaker result than Theorem 3.6 had already been established earlier in [9]. In contrast, the version presented above furnishes additional upper bounds on the norm of the solution paths at the time $t_{0,\varepsilon}$, which is crucial for the result on the second phase of the decomposition process.

Before we move on to the second decomposition stage, let us briefly comment on the differences between Theorem 3.6 and the corresponding result for the Cahn-Hilliard model (1). The above result is closest in spirit to the studies in [48, 49] — yet the approaches and proof techniques differ considerably. As we mentioned before, the homogeneous state $\bar w \equiv m$ is an equilibrium in the deterministic case, i.e., spinodal decomposition

can only be observed by considering non-homogeneous initial conditions. However, not all initial conditions close to the homogeneous state lead to spinodal decomposition. Thus, one has to identify suitable initial conditions that lead to phase separation, and then show that the set of these initial conditions is large. In [48, 49], the former problem is solved by determining a power law shaped region near $\bar{w}$ containing the appropriate initial conditions. Using a tangency property of the power law, one can then show that on small balls around $\bar{w}$ the size of the set of initial conditions leading to spinodal decomposition is large compared to its complement.

Nevertheless, the results in [48, 49] have several drawbacks. For technical reasons, the results were obtained by considering a finite-dimensional inertial manifold which contains the homogeneous state. The measure theoretic part concerning the size of the set of appropriate initial conditions uses a Lebesgue measure on this manifold. Even though it is shown that solutions outside the inertial manifold converge exponentially fast to it, all results are stated in terms of the finite-dimensional projection of the solutions, and not in terms of the full infinite-dimensional phase space of (1). Furthermore, the deterministic result allows for initial conditions arbitrarily close to the homogeneous state. This implies that there is no common time frame for the first decomposition stage. In fact, it was pointed out in [30, 48] that initial conditions which are too close to the homogeneous state can lead to nonphysical dynamical behavior. We will address this point in more detail in Section 3.4, where recent results describing the evolution of the pattern complexity will be discussed. Finally, while the results in [48, 49] identify appropriate initial conditions that lead to spinodal decomposition, there is no intrinsic selection mechanism for the physically relevant initial states in the deterministic model.

The situation is different for the stochastic case discussed above. Now the result addresses spinodal decomposition in the full infinite-dimensional phase space, it furnishes a common time frame for the pattern generation, and the additive noise term provides an intrinsic selection mechanism for the observed patterns.

3.3 Second Decomposition Stage

As we mentioned in Section 3.1, the first stage of spinodal decomposition does select the complicated patterns characteristic for this phase separation phenomenon. Yet, at the end of the first stage the amplitude of the patterns, i.e., the $L^\infty(G)$-norm of $u(t_{0,\varepsilon})$, is still small. In contrast, numerical simulations indicate that these patterns more or less persist while the maximum norm of u grows, until the norm reaches an ε-independent threshold. This growth phase constitutes the second stage of spinodal decomposition, and for the deterministic Cahn-Hilliard model it was studied in [57, 58]. For the stochastic model a description has been obtained only recently in [10] — and this description will be presented in more detail in the remainder of this section.

Consider again the stochastic solution process u of the initial value problem (22), and recall the stochastic event $\mathcal{N}_{1,\varepsilon}$ defined in (27). In order to describe the second decomposition stage, we define the event

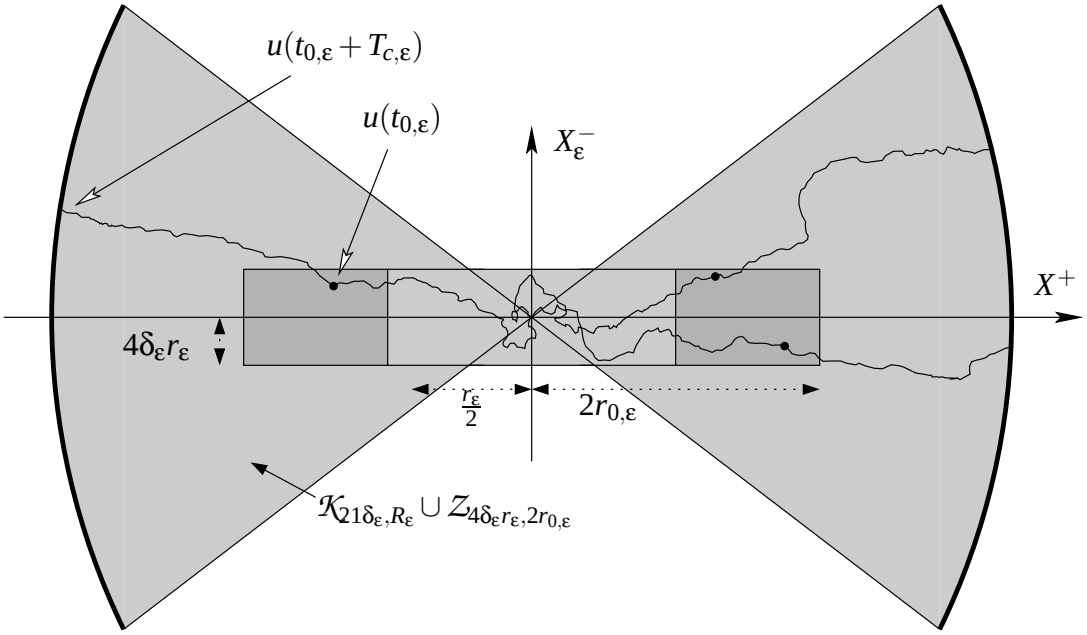

Figure 6: A sketch of three typical trajectories on $\mathcal{S}_\varepsilon$.

$$\mathcal{N}_{2,\varepsilon} := \left\{ u(t+t_{0,\varepsilon}) \in \mathcal{K}_{21\delta_\varepsilon,R_\varepsilon} \quad \text{for all} \quad t \in [0,T_{c,\varepsilon}] \,, \quad \|u(t_{0,\varepsilon}+T_{c,\varepsilon})\|_* = R_\varepsilon \right\} \,,$$

where $t_{0,\varepsilon}+T_{c,\varepsilon}$ denotes the first exit time of u from the truncated cone $\mathcal{K}_{21\delta_\varepsilon,R_\varepsilon}$ after $t_{0,\varepsilon}$. In this definition, the time $t_{0,\varepsilon}$ denotes the deterministic end time of the first decomposition stage as in (27), and δ_ε is the small positive number defined in (28). The cone $\mathcal{K}_{21\delta_\varepsilon,R_\varepsilon}$ was introduced in Definition 3.3. Since we are interested in solution trajectories which exhibit both stages of spinodal decomposition, we further define

$$\mathcal{S}_\varepsilon := \mathcal{N}_{1,\varepsilon} \cap \mathcal{N}_{2,\varepsilon} \,. \tag{29}$$

Typical solution trajectories corresponding to the event $\mathcal{S}_\varepsilon$ are shown in Figure 6. We would like to point out that for the sake of readability, the figure does not correctly reproduce the true size relations. The opening of the cone is determined by the constant δ_ε defined in (28). Thus, the cone is actually an extremely narrow cone around the dominating subspace X_ε^+, and therefore solutions in $\mathcal{K}_{21\delta_\varepsilon,R_\varepsilon}$ exhibit the patterns of functions in X_ε^+. Moreover, the radius R_ε up to which we can describe the second decomposition phase will be extremely large compared to $r_\varepsilon < r_{0,\varepsilon}$.

The following result is taken from [10, Theorem 4.13]. It shows that the probability of the event $\mathcal{S}_\varepsilon$ is close to 1 for small ε. In fact, for $\varepsilon \to 0$ the probability converges to 1 faster than any polynomial in ε. The result is stated in terms of fairly complicated conditions on r_ε, σ_ε and R_ε, which will be discussed in more detail afterwards.

Theorem 3.7 *Let u denote the mild solution of the stochastic initial value problem (22), and consider the situation of Theorem 3.6. In addition to the assumptions of Theorem 3.6, suppose that for a small positive constant ζ_3 we have*

(S3) $\lim_{\varepsilon\to 0} r_\varepsilon^{-\tilde\rho}\cdot\delta_\varepsilon^{\kappa-1}\cdot R_\varepsilon^{\kappa+\tilde\rho}\cdot\Theta_\varepsilon^{(1-\gamma^+)/(2\gamma^+)}=0$, *where* $\tilde\rho:=(1+\zeta_3-\gamma)/\gamma>0$, *as well as*

(S4) $\lim_{\varepsilon\to 0} R_\varepsilon\cdot\delta_\varepsilon=0$, *and*

(S5) $\lim_{\varepsilon\to 0} r_\varepsilon\cdot R_\varepsilon^{-1}\cdot\Theta_\varepsilon^{(1-\gamma^+)/(2\gamma^+)}=0$ *(which is equivalent to $r_\varepsilon<r_{0,\varepsilon}<R_\varepsilon$).*

Then for any $q>0$ there exists a constant $C_q>0$ such that

$$\mathbb{P}(\mathcal{S}_\varepsilon^c)\le C_q\cdot\varepsilon^q$$

for all sufficiently small $\varepsilon>0$, where $\mathcal{S}_\varepsilon$ was defined in (29).

Proof outline: Similar to the proof of Theorem 3.6, the result on the second decomposition stage is achieved by relating the dynamics of the nonlinear solution u of (22) to the linearized stochastic dynamics given by (11). This time, however, it is not sufficient to relate the dynamics to the solution $\sigma_\varepsilon\cdot W_{A_\varepsilon}(t)$, which originates at the origin. Rather, we have to consider the solution $v(t)$ of (11) satisfying $v(0)=u(t_{0,\varepsilon})$. At this point, it is convenient that the end time $t_{0,\varepsilon}$ of the first decomposition stage is deterministic. This fact implies that we can represent v as

$$v(t)=e^{tA_\varepsilon}u(t_{0,\varepsilon})+\sigma_\varepsilon\cdot\widetilde{W}_{A_\varepsilon}(t)\,,$$

where $\widetilde{W}_{A_\varepsilon}$ denotes the stochastic convolution with respect to the shifted Q-Wiener process $\widetilde{W}(t)=W(t+t_{0,\varepsilon})-W(t_{0,\varepsilon})$, $t\ge 0$. Furthermore, one can show that

$$u(t+t_{0,\varepsilon})=e^{tA_\varepsilon}u(t_{0,\varepsilon})+\widetilde{W}_{A_\varepsilon}(t)+\int_0^t e^{(t-\tau)A_\varepsilon}F(u(\tau+t_{0,\varepsilon}))\,d\tau\quad\text{for}\quad t\ge 0\,,$$

and that both W_{A_ε} and $\widetilde{W}_{A_\varepsilon}$ have the same distributions.

Using this setting, the first part of the proof of Theorem 3.7 consists of introducing a stochastic event $\Omega_{2,\varepsilon}$ defined in terms of exponential growth conditions for the stochastic convolution $\widetilde{W}_{A_\varepsilon}$. Combined with the nonlinearity estimate

$$\|F(u)\|_{L^2(G)}\le C\cdot\delta_\varepsilon^\kappa\cdot\|u\|_*^{1+\kappa}\qquad\text{for all}\qquad u\in\mathcal{K}_{21\delta_\varepsilon,R_\varepsilon}\,,\tag{30}$$

which was derived in [58], one can then show that the relative distance of the nonlinear solution trajectory u and the linear solution v satisfies

$$\frac{\|u(t+t_{0,\varepsilon})-v(t)\|_*}{\|v(t)\|_*}\le\delta_\varepsilon\qquad\text{for all}\qquad 0\le t\le T_{c,\varepsilon}\,.\tag{31}$$

In other words, the solution u follows v closely on the set $\Omega_{2,\varepsilon}$, and this can be used to establish the inclusion $\Omega_{1,\varepsilon}\cap\Omega_{2,\varepsilon}\subset\mathcal{S}_\varepsilon$.

The second part of the proof consists of determining a lower bound on the probability of the event $\Omega_{2,\varepsilon}$. By using the fact that both W_{A_ε} and $\widetilde{W}_{A_\varepsilon}$ have the same distributions, this step can basically be reduced to the second step of the proof of Theorem 3.6. $\diamond$

The above result gives a precise description of both decomposition stages by relating the dynamics of u to the linearized dynamics. Moreover, the characteristic spinodal decomposition patterns are a consequence of the closeness of $u(t)$ to the dominating subspace X_ε^+ for $t_{0,\varepsilon} \le t \le t_{0,\varepsilon} + T_{c,\varepsilon}$. For more details, see [48, Section 4].

To close this section, let us discuss the fairly involved conditions in Theorems 3.6 and 3.7. In particular, we would like to demonstrate which radii R_ε can be achieved for various values of κ. For the sake of simplicity, assume that the relevant ε-dependent quantities are given as powers of ε in the form

$$r_\varepsilon = \varepsilon^{\varphi_r}\,, \qquad R_\varepsilon = \varepsilon^{\varphi_R}\,, \qquad \text{and} \qquad \sigma_\varepsilon = \varepsilon^{\varphi_\sigma}\,.$$

Then the auxiliary variable Θ_ε defined in (24) satisfies $\Theta_\varepsilon = \varepsilon^{\varphi_\Theta}$, where

$$\varphi_\Theta \;=\; 2\varphi_r - 2\varphi_\sigma - 2s_* + d + 2 \;=\; 2\varphi_r - 2\varphi_\sigma - D\,.$$

Using the definition of δ_ε in (28), one can then easily show that (S1) through (S5) are equivalent to

$$\varphi_\Theta \;<\; -\frac{2\gamma^+}{\gamma^+ - \tilde\gamma}\cdot\left(2-\frac{d}{2}\right)\,, \tag{32}$$

$$\varphi_r \;>\; \frac{1-\kappa}{\kappa}\cdot\left(2-\frac{d}{2}\right) - \frac{1+2\tilde\kappa}{2\kappa}\cdot\varphi_\Theta\,, \tag{33}$$

$$\varphi_R \;>\; \frac{1-\kappa}{\kappa+\tilde\rho}\cdot\left(2-\frac{d}{2}\right) + \frac{\tilde\rho}{\kappa+\tilde\rho}\cdot\varphi_r - \frac{1-\gamma^+}{2\gamma^+(\kappa+\tilde\rho)}\cdot\varphi_\Theta\,, \tag{34}$$

$$\varphi_R \;>\; -\left(2-\frac{d}{2}\right)\,, \tag{35}$$

$$\varphi_R \;<\; \varphi_r + \frac{1-\gamma^+}{2\gamma^+}\cdot\varphi_\Theta\,. \tag{36}$$

We are mainly interested in the exponents φ_R, φ_σ, and s_*. To simplify our considerations, we assume that $m = 0$ and $f(u) = u - u^{1+\kappa}$ in Theorem 3.7. Then the optimal values of φ_R can be determined as follows:

- Using (32), choose and fix the quantity φ_Θ. The best possible value for φ_R can be achieved by choosing φ_Θ as large as possible, i.e.,

  $$\varphi_\Theta \;\lessapprox\; -\frac{2\gamma^+}{\gamma^+ - \tilde\gamma}\cdot\left(2-\frac{d}{2}\right)\,,$$

  which generally is a large negative number.

- Next, use (33) to choose and fix the auxiliary exponent φ_r as

$$\varphi_r \gtrapprox \left(\frac{1-\kappa}{\kappa}+\frac{\gamma^+(1+2\tilde{\kappa})}{\kappa(\gamma^+-\tilde{\gamma})}\right)\cdot\left(2-\frac{d}{2}\right),$$

  which is a large positive number.

- The remaining estimates (34), (35), and (36) now determine the possible range for φ_R. One can easily show that the optimal choice of φ_R implied by (34) is given by

$$\varphi_R \gtrapprox \left(\frac{1-\kappa}{\kappa+\tilde{\rho}}+\frac{\tilde{\rho}\gamma^+(1+2\tilde{\kappa})}{\kappa(\kappa+\tilde{\rho})(\gamma^+-\tilde{\gamma})}+\frac{\tilde{\rho}(1-\kappa)}{\kappa(\kappa+\tilde{\rho})}+\frac{1-\gamma^+}{(\gamma^+-\tilde{\gamma})(\kappa+\tilde{\rho})}\right)\cdot\left(2-\frac{d}{2}\right),$$

  and that the remaining bounds (35) and (36) can then be achieved as well.

- The order of magnitude for the noise intensity exponent φ_σ is given by

$$\varphi_\sigma \gtrapprox -\frac{D}{2}+\left(\frac{1-\kappa}{\kappa}+\frac{\gamma^+(1+\kappa+2\tilde{\kappa})}{\kappa(\gamma^+-\tilde{\gamma})}\right)\cdot\left(2-\frac{d}{2}\right).$$

  This expression is generally a large positive number, which effectively limits the allowable intensity of the noise process.

By choosing the parameters $\gamma<\tilde{\gamma}<\gamma^+<1$ close enough to 1, as well as choosing $\tilde{\kappa}>0$ and $\tilde{\rho}>0$ sufficiently small, the expression for φ_R can be simplified significantly. The last two terms in parentheses can be made arbitrarily small. Moreover, due to the definition of $\tilde{\rho}$ in Theorem 3.7, the expression $\tilde{\rho}\gamma^+/(\gamma^+-\tilde{\gamma})$ is always bigger than 1, yet it can be chosen arbitrarily close to 1. Altogether, one obtains

$$\varphi_R \gtrapprox \left(-1+\frac{1}{\kappa}+\frac{1}{\kappa^2}\right)\cdot\left(2-\frac{d}{2}\right). \tag{37}$$

In other words, our main Theorem 3.7 describes the dynamics of spinodal decomposition in the stochastic Cahn-Hilliard-Cook equation (22) until the solution u reaches distances of the order ε^{φ_R} from the homogeneous state, where φ_R is given by (37). Notice that for $\kappa\geq 2$ this order becomes unbounded for $\varepsilon\to 0$. This at first sight strange fact is a consequence of the underlying norm. Our studies are performed in the phase space $X^{1/2}\subset H^2(G)$ equipped with the norm $\|\cdot\|_*$ defined in Section 2.2, which is equivalent to the standard $H^2(G)$-norm. Thus, the norm includes a measure of curvature — and for the extremely irregular spinodally decomposed states this implies large values of the norm.

From a physical point of view, one is of course interested in the amplitude of the solution u, i.e., its $L^\infty(G)$-norm. It was shown in [49] that passing from the $H^2(G)$-norm to the maximum norm for functions near X_ε^+ can be achieved by the multiplicative factor ε^2. In other words, our main result describes the dynamics of spinodal decomposition until

the maximum norm of the solution u reaches an order of $\varepsilon^{2+\varphi_R}$. For large values of κ, we can therefore achieve orders close to $\varepsilon^{d/2}$ for the maximum norm. Even though this order is smaller than the anticipated ε-independent constant, it is a significant improvement of earlier results.

How do our stochastic results compare to the deterministic result in [58]? The exponent φ_R in (37) is slightly worse than the one obtained in the deterministic case, which furnished an exponent of

$$\varphi_R \stackrel{>}{\approx} \left(-1+\frac{1}{\kappa}\right)\cdot\left(2-\frac{d}{2}\right). \tag{38}$$

However, for large values of κ the deviation is very small. In addition, our stochastic result provides the first description of the complete decomposition process, including a satisfactory explanation of the transition between the two stages.

3.4 Further Discussion and Possible Extensions

The results on the two stages of spinodal decomposition described in Sections 3.2 and 3.3 provide a clear picture of instantaneous phase separation in the Cahn-Hilliard-Cook model. Yet, these results do not tell the complete story. First of all, we already pointed out that the end of the second stage in Theorem 3.7 occurs too early. The pattern amplitude at this point is still small in ε, even though one would expect an ε-independent threshold. *Is it possible to obtain a complete description of the second stage?* Our results also raise a more fundamental question. Both the deterministic and the stochastic results on spinodal decomposition relate the nonlinear dynamics to the linearized dynamics. This fact is of course not surprising, since both approaches rely on properties of the nonlinearity — and the nonlinearity remains the same for both models. Moreover, both results explain the pattern morphology by the closeness of the linear evolution to the dominating subspace X_ε^+. While we did describe differences between the deterministic and the stochastic results at the end of Sections 3.2 and 3.3, these were mainly technical in nature. *Do the results differ in more essential aspects?* In the following, we address both of these questions in more detail.

(a) Toward a complete description of the second decomposition stage.

Theorem 3.7 and its deterministic counterpart in [58] mark a big step toward explaining the second stage of spinodal decomposition. They establish linear behavior in the respective model until the $H^2(G)$-norm of the solution u reaches a distance proportional to ε^{φ_R}, for small $\varepsilon > 0$. Yet, as we pointed out above, the exponent φ_R, given by (37) in the stochastic case and by (38) in the deterministic case, falls short of the numerically determined exponent -2. For more details we refer the reader to [54, 57].

Nevertheless, even a quick glance at the specifics of the above results shows that there is considerable room for improvement. The nonlinear evolution is linked to the linear evolution by establishing the smallness of the relative distance in (31) — and at the end of the second stage, this distance is proportional to $\varepsilon^{2-d/2}$. Since it would be enough to show

that the relative distance is bounded by a sufficiently small ε-independent constant, it seems reasonable to hope that an iterative application of the techniques in [10, 58] would furnish the desired order.

Unfortunately, the situation is more complicated than that. To make this clear, we consider the deterministic result in [58]. This result indicates that as the dimension of the domain G increases, the radius to which linear behavior can be observed decreases significantly. In fact, both the exponent φ_R in (38) and the bound on the relative distance in (31) are worse for higher dimensions. This dimension-dependence is in stark contrast to the numerically observed exponent $\varphi_R \approx -2$ which is dimension-independent.

A natural starting point for any attempt to improve the result of [58] is therefore a test of its optimality. For $G = (0,1)^2$, $m = 0$, and $f(u) = u - u^3$, i.e., $\kappa = 2$, such a test can be found in the introduction of [65]. By following linear and nonlinear solutions originating at randomly chosen initial conditions close to 0 until their relative distance exceeds $\varepsilon/9$, and then recording the $H^2(G)$-norm of the nonlinear solution, one can obtain a numerical estimate for the optimal exponent φ_R subject to the constraint (31). The simulation results for various ε-values in [65, Figure 2] furnish $\varphi_R \approx -3/2$, which is considerably smaller than the exponent $\varphi_R \approx -1/2$ predicted by (38). These simulations seem to indicate that [58] is highly sub-optimal in two dimensions, and that the estimates of [58] are not sharp.

As it turns out, the above indication is false. Wanner [65] was able to construct a family of functions $w_\varepsilon \in X_\varepsilon^+$ which establishes the optimality of the crucial nonlinearity estimate in [58]; this estimate is stated in (30). In addition, if one repeats the above numerical experiment starting at small multiples of these functions w_ε, then the exponent φ_R is numerically confirmed as $-1/2$.

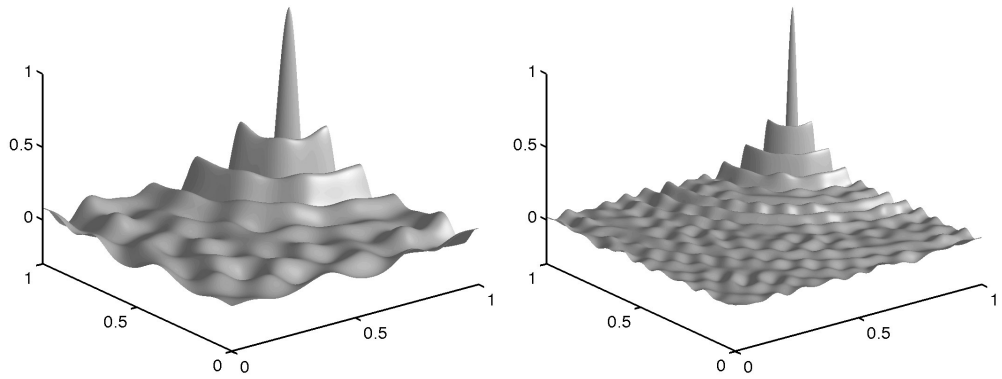

Figure 7: Functions in the dominating subspace X_ε^+ which establish the optimality of (30). In each case we use $\gamma = 0.95$ in Definition 3.2. The left diagram is for $\varepsilon = 0.02$ and $\dim X_\varepsilon^+ = 49$; the right diagram is for $\varepsilon = 0.01$ and $\dim X_\varepsilon^+ = 183$.

The numerical results presented in the introduction of [65] show that there is no hope of universally improving the results in [58]. Yet, a closer look at the shape of the functions w_ε establishing the optimality of (30) points to a possible solution. Figure 7 shows the

function w_ε for $G=(0,1)^2$ and two different ε-values. While these functions are contained in the dominating subspace X_ε^+, their patterns do not resemble the ones normally observed during spinodal decomposition. The functions w_ε exhibit a very localized structure, which is not shared by the majority of functions in or close to X_ε^+. One can therefore hope that by excluding functions of this type, the result of [58] can be improved.

For the deterministic Cahn-Hilliard equation (1), the results in [65] achieve exactly this for one-, two-, and three-dimensional rectangular domains. By excluding a small subset of a cone around X_ε^+, one can show that the nonlinearity estimate (30) can be improved significantly, with δ_ε being replaced by the dimension-independent quantity

$$\delta_\varepsilon^* = \delta_0 \cdot \varepsilon^2 \cdot \sqrt{|\ln \varepsilon|}\,. \tag{39}$$

This improvement uses results on Fourier series with random coefficients in order to quantify the size of the excluded subset. Based on the new nonlinearity estimate, one can then prove the following main result of [65].

Theorem 3.8 *Consider the deterministic Cahn-Hilliard equation (1) on a rectangular domain G in $\mathbb{R}^d$, where $d \in \{1,2,3\}$, and assume $f'(m) > 0$. Suppose that Assumption 2.9 is satisfied, and let $\rho > 0$ be arbitrarily small, but fixed. In addition, consider an initial condition w_0 close to the homogeneous state $\bar{w} \equiv m$ such that $w_0 - m$ is sufficiently close to the dominating subspace X_ε^+ defined in Definition 3.2. Finally, let w denote the solution of (1) starting at w_0, and let $v(t) = e^{tA_\varepsilon}(w_0 - m)$ denote the solution of the linearized Cahn-Hilliard equation starting at $w_0 - m$. Then for most such initial conditions w_0, as long as*

$$\|w(t) - m\|_* \le C \cdot \varepsilon^{-2+\rho+2/\kappa} \cdot \|w_0\|_*^\rho\,,$$

we have

$$\frac{\|w(t) - v(t) - m\|_*}{\|v(t)\|_*} \le \delta_\varepsilon^*\,.$$

The dimension-independent bound δ_ε^* was defined in (39).

For more details we refer the reader to [65, Theorem 4.7]. The above result shows that linear behavior determines the dynamics of (1) until the nonlinear solution reaches a distance proportional to $\varepsilon^{\varphi_R^*}$ from the homogeneous state, with the dimension-independent exponent

$$\varphi_R^* \;\gtrapprox\; -2 + \frac{2}{\kappa}\,.$$

For large values of κ, Theorem 3.8 therefore furnishes the dimension-independent exponent -2 which was observed in numerical simulations. In view of the smallness of δ_ε^* and its dimension-independence, a complete description of the second decomposition stage for arbitrary f seems to be within reach as well, at least for the deterministic model. As mentioned above, such a description can probably be obtained by an iterative application of the estimates in [65]. It remains to be seen whether it is possible to adapt these results to the stochastic case.

(b) Pattern complexity evolution during spinodal decomposition.

We now turn our attention to the second question raised in the beginning of this subsection: Are there any fundamental differences between the deterministic model (1) and the stochastic model (3) concerning spinodal decomposition? The results described so far explain spinodal decomposition by the dynamics of the linearized model — and even though the linearized models in the deterministic and the stochastic case differ by an additive noise term, both appear to qualitatively reproduce the complicated patterns observed during spinodal decomposition.

It is not immediately clear how one can characterize these complicated patterns in a more quantitative way. Due to the complete lack of any symmetry or periodicity, most standard methods do not seem to be applicable. One possible approach has been proposed recently in [30, 40] and is based on algebraic topology, in particular, homology theory. Consider a solution $w(t)$ of either (1) or (3) at time t, and assume that $w(0)$ is either equal or close to the homogeneous state m in the spinodal interval. Then we can define the set

$$M(t) = \{x \in G \,:\, w(t,x) > m\} \subset G \qquad \text{for all} \qquad t \geq 0\,,$$

which describes the microstructure formed by $w(t)$. For one-dimensional domains G, this set generally consists of several components, and the number of components can be viewed as a coarse measure of the complexity of $w(t)$. Similarly, in two and three space dimensions one can study the number of components of $M(t)$ as a quantitative measure for the complexity of the microstructure. In Figure 8 we depict two sets $M(t)$ generated through spinodal decomposition for the two-dimensional domain $G = (0,1)^2$. The left microstructure was generated by the deterministic Cahn-Hilliard model (1), the right one is a realization of the stochastic model (3). One can show that the left pattern consists of 61 components, while the right pattern has only 34 components. Yet, in the higher-dimensional setting, additional quantities are of interest. It can easily be seen that both microstructures in Figure 8 form loops. In fact, the left microstructure has exactly 14 loops, while the right one has only 7.

But, what exactly do the above numbers tell us about the patterns shown in Figure 8? From a qualitative point of view, both patterns appear similar. The only visible difference is that the right pattern seems coarser than the left one — and this is one of the facts captured by the number of components or loops.

From a mathematical point of view, the microstructure $M(t) \subset G$ is nothing but a topological space with respect to the topology induced by G. As such, we can use topological invariants which capture only the essential topological information in our study of $M(t)$. In homology theory, such invariants are given by abelian groups $H_k(M(t))$ for $k \in \mathbb{Z}$, as well as certain integral quantities derived from them. We are particulary interested in the so-called Betti numbers. The k-th Betti number of the topological space $M(t)$ is defined as the rank of the free subgroup of the k-th homology group $H_k(M(t))$. Despite their abstract definition, these numbers have a straightforward interpretation. The zeroth Betti number is precisely the number of components of $M(t)$. Similarly, the first Betti number counts the number of nontrivial independent loops in $M(t)$, i.e., loops that cannot be contracted to a point within $M(t)$ or morphed into each other.

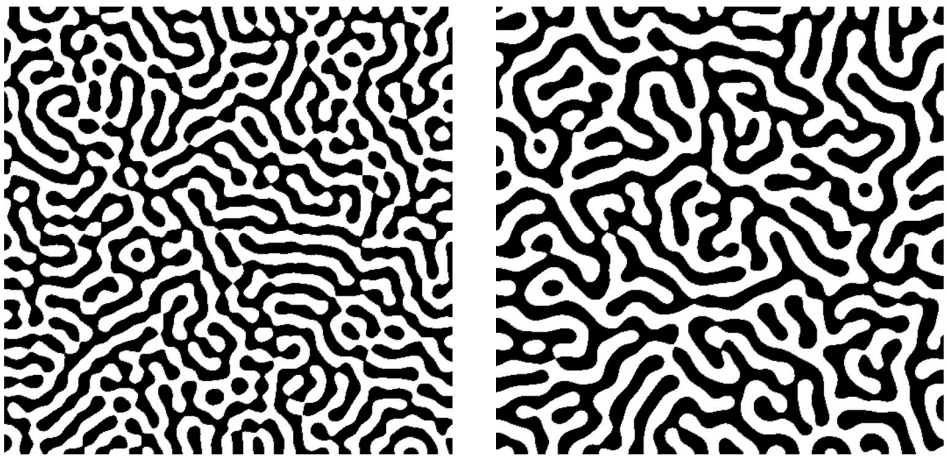

Figure 8: Two-dimensional microstructures $M(t)$ generated through spinodal decomposition for $G = (0,1)^2$, $\varepsilon = 0.005$, and $t = 0.0015$. The left structure was generated by the deterministic model, the right one by the stochastic model for $\sigma_\varepsilon = 0.01$.

Having identified coarse, but quantitative, measures for the complexity of a microstructure, we return to the question posed in the beginning. Are there any essential differences between the spinodal decomposition dynamics of (1) and (3)? One possible approach would be to consider solutions of either model starting at random initial conditions close to the homogeneous state, and determine the temporal evolution of the Betti numbers of $M(t)$. By considering ensembles of solutions, it is then possible to compute averaged complexity evolution curves which are in some sense characteristic for each model. This numerical approach has been implemented in [30], based on computational homology software associated with [40]. The results of this study are surprising and point toward a distinct difference between the models. In both models, the smoothing effect of the parabolic equation causes a rapid complexity decrease during the initial evolution from the highly irregular initial condition. For the stochastic model subject to sufficiently strong noise, this monotone decrease continues throughout the spinodal decomposition phase. In contrast, the complexity of the patterns generated by the deterministic model (1) starts to grow again, leading to finer microstructures. Only at the end of the spinodal decomposition phase — when coarsening sets in — does the complexity fall again. This difference in complexity can easily be seen in the microstructures of Figure 8. For more details we refer the reader to [30] or [40, Sections 1.1 and 8.2].

The results of [30] indicate that there are considerable differences between the spinodal decomposition patterns of the deterministic and the stochastic Cahn-Hilliard model. Therefore, it is only natural to wonder which of the two models is more appropriate. Recent advances in experimental methods have allowed materials scientists to obtain high-resolution images of decomposing metal alloys. For example, spinodal decomposition in iron-chromium alloys has been studied in [50, 37, 38]. In particular, the last part of this

three-paper series is concerned with topological properties of the generated microstructures. The authors determine the temporal evolution of the handle density of the microstructure, which corresponds to its first Betti number. The due to the enormous experimental effort limited results in [38] indicate that this topological quantity decays monotonically as time increases. In other words, for the specific situation considered in [50, 37, 38], the stochastic model appears to be more adequate than the classical deterministic Cahn-Hilliard equation.

4 Nucleation

Spinodal decomposition is only one of the two main phase separation phenomena described by the Cahn-Hilliard models. In this section, we address the second phenomenon, namely nucleation. We describe known results for the deterministic equation in Section 4.1. These considerations naturally lead to questions concerning the structure of the global attractor of the deterministic Cahn-Hilliard model, which will be addressed briefly in Section 4.2. However, it is our belief that a complete description of nucleation is only possible in the stochastic setting. This is outlined in Section 4.3.

4.1 Nucleation in the Deterministic Model

Throughout this subsection we consider the deterministic Cahn-Hilliard equation (1). It has already been mentioned in the introduction that the dynamics of this partial differential equation for initial conditions close to the homogeneous state m depends crucially on the sign of $f'(m)$. In the case $f'(m) > 0$, the homogeneous state is unstable, and this fact leads to spinodal decomposition as described in the previous section. In contrast, for $f'(m) < 0$ the homogeneous state is asymptotically stable, i.e., orbits starting close to the homogeneous state will converge to it as $t \to \infty$. It is therefore somewhat surprising that even in this latter case one can observe phase separation dynamics.

In their seminal paper [3], Bates and Fife address the problem of nucleation for the case of one-dimensional domains G. Assuming $f'(m) < 0$, they establish the following results for the Cahn-Hilliard equation (1):

- The constant function $\bar{w} \equiv m$ is an asymptotically stable equilibrium of (1).
- There exists an equilibrium solution w_{global} of (1) which is a global minimizer of the energy (2), and which has lower energy than $\bar{w}$. This solution exhibits one sharp transition layer between the pure states $w = -1$ and $w = +1$.
- In addition, there is an unstable equilibrium solution w_{nuc} of index 1, whose one-dimensional unstable manifold limits to $\bar{w}$ and w_{global}, respectively. This solution is almost everywhere close to m, but it exhibits a small amplitude spike near the boundary of the one-dimensional domain G.

If the homogeneous equilibrium $\bar{w}$ is perturbed beyond the *critical nucleus* w_{nuc}, then the solution of (1) will follow its unstable manifold and converge to the decomposed global

energy minimizer w_{global}. See also the diagram in Figure 9. Moreover, the necessary perturbation is relatively small in the sense that it is localized at the boundary of the domain and of a small amplitude. Bates and Fife also describe the actual phase separation dynamics as the solution of (1) follows the unstable manifold of the critical nucleus. Thus, their results provide a clear and convincing explanation of the dynamics of nucleation in one space dimension — once the initial perturbation has been introduced.

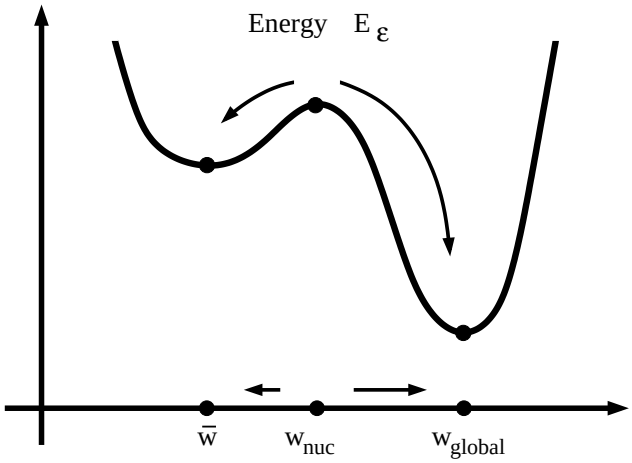

Figure 9: Schematic energy diagram: The homogeneous equilibrium $\bar{w}$, the canonical nucleus w_{nuc}, and the global minimizer w_{global}.

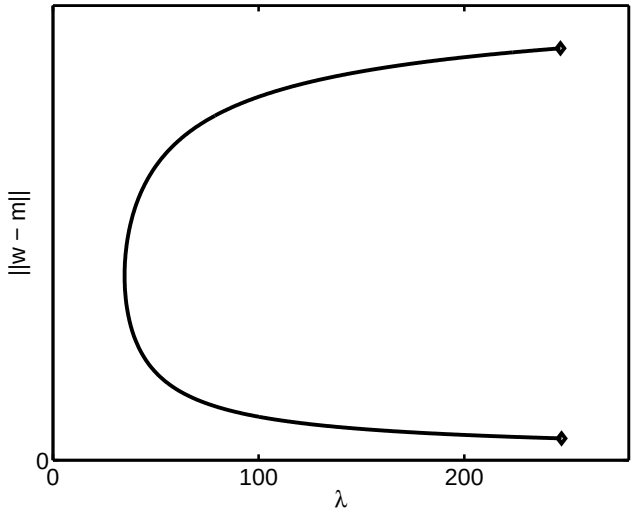

Figure 10: Continuum of equilibrium solutions for the deterministic Cahn-Hilliard equation for mass $m = -0.6$ and $G = (0,1)^2$, with $\lambda = 1/\varepsilon^2$.

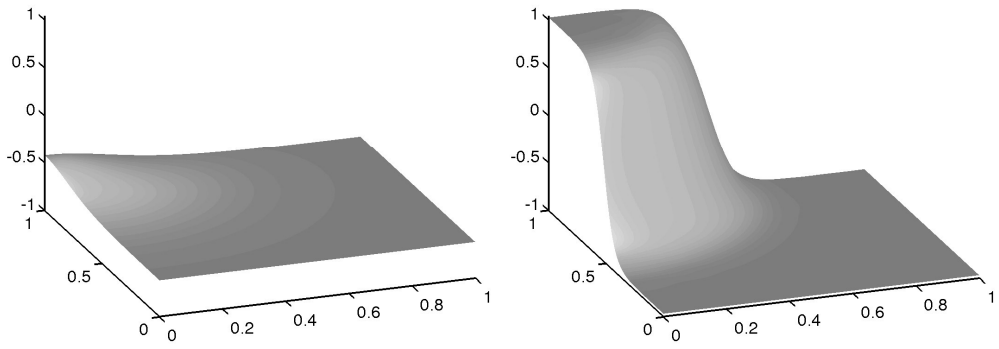

Figure 11: The canonical nucleus (left diagram) and the corresponding global minimizer (right diagram) for $G = (0,1)^2$ and $\varepsilon = 0.0637$, or $\lambda = 25\pi^2$.

The basic picture described in [3] can probably be carried over to the case of higher-dimensional domains as well. Numerical results for two-dimensional rectangular domains have produced solution branches of equilibrium solutions as shown in Figure 10 which are created through saddle-node bifurcations. While the equilibria on the upper branch are stable, the equilibria on the lower branch have a one-dimensional unstable manifold. Furthermore, in the limit $\varepsilon \to 0$, the solutions on the lower branch converge to the homogeneous equilibrium m. It seems plausible to assume that for each value of ε, the equilibrium on the lower branch is a critical nucleus, and the one on the upper branch represents the global energy minimizer — and a look at the equilibria shown in Figure 11, which correspond to the diamonds in Figure 10, reinforces this assumption. For more details on the involved numerical methods we refer the reader to [21, 44].

Mathematically rigorous results for higher-dimensional domains are mainly concerned with identifying equilibrium solutions which can serve as canonical nuclei, and discussing their stability properties. See for example [2, 4, 5, 53, 66, 67, 68]. To the best of our knowledge, higher-dimensional dynamical results analogous to the study in [3] are not available at this time.

4.2 Deterministic Attractor Structure

The results of [3] highlight significant differences between the study of spinodal decomposition and nucleation in the deterministic Cahn-Hilliard model. While the study of spinodal decomposition is essentially aimed at understanding transient dynamics far from any non-trivial equilibrium solution of (1), the study of nucleation depends critically on a profound understanding of the structure of the equilibrium set. Moreover, in order to understand the droplet growth during nucleation, one has to describe the dynamics along certain heteroclinic solutions of (1). In this way, the study of nucleation leads naturally to a study of the global attractor of the Cahn-Hilliard equation, whose existence was established in [55], see also [61].

The first step in studying the attractor of any evolution equation consists in understanding the set of its equilibrium solutions. For the one-dimensional Cahn-Hilliard model, this has been accomplished completely only recently by Grinfeld and Novick-Cohen [32]. For higher-dimensional base domains only partial results are available. On the one hand, these are results targeting specific types of equilibria for general domains G, such as the spike solutions mentioned in Section 4.1. In addition, there are a number of studies aimed at describing the complete bifurcation structure, but for specific simple domains G such as rectangles. See for example [26, 41, 42, 47]. Recent numerical studies indicate that even for the case of the unit square $G = (0,1)^2$ a complete, rigorous description of the set of equilibria is currently out of reach [44, 45], and that one has to resort to the use of computer-assisted proofs similar to the ones in [34, 60, 69, 70].

In order to describe the flow on a compact attractor, Conley [16] introduced the notion of Morse decomposition, which decomposes the attractor into invariant sets called Morse sets and connecting orbits between them. For gradient systems such as the Cahn-Hilliard equation, the Morse sets correspond to the equilibrium solutions. Obtaining a description of the Morse decomposition of an attractor in particular examples may be difficult, although it has been achieved completely in several cases. One particularly promising approach based on Conley's connection matrix [27, 28] is due to Mischaikow [51, 52], and has already been applied successfully to several partial differential equation models, including the one-dimensional Cahn-Hilliard equation [33, 52]. Extending these results to higher-dimensional domains relies crucially on an understanding of the set of equilibria, in particular their stability properties. Only partial results are available at this time [45, 46].

4.3 Toward a Theory of Stochastic Nucleation

The explanation of nucleation in the deterministic Cahn-Hilliard model due to Bates and Fife [3] gives a detailed description of the process — once the initial state has been perturbed to an initial condition outside the domain of attraction of the stable homogeneous state. Unfortunately, however, the results of [3] do not address the question of how the initial perturbation is generated, or when. Yet these are questions of crucial importance for materials design. How long does it take before the first droplet nucleates? If this time frame exceeds certain thresholds, one might still be able to characterize the material as stable for all practical purposes. It is therefore necessary to consider a model for nucleation which intrinsically can describe the mechanism responsible for the appearance of the droplets, and the deterministic Cahn-Hilliard model (1) is not capable of such a description.

On an intuitive level, the Cahn-Hilliard-Cook model can easily describe the mechanism responsible for nucleation. The random force $\sigma_{\text{noise}} \cdot \xi$ in the right-hand side of (3) will perturb the composition of the alloy away from the homogeneous state $\overline{w} \equiv m$, which, as we already pointed out, is no longer an equilibrium solution. While in the short term this will not significantly affect the material, the cumulative effect of these perturbations can cause the function w to reach the boundary of the domain of attraction of $\overline{w}$, and to eventually enter the domain of attraction of a state with lower energy. Depending on the strength of the noise, which in turn is determined by σ_{noise}, this domain exit takes place sooner or later.

In addition, one would expect that the solution can exit the domain of attraction at a variety of points — leading to different nucleation patterns.

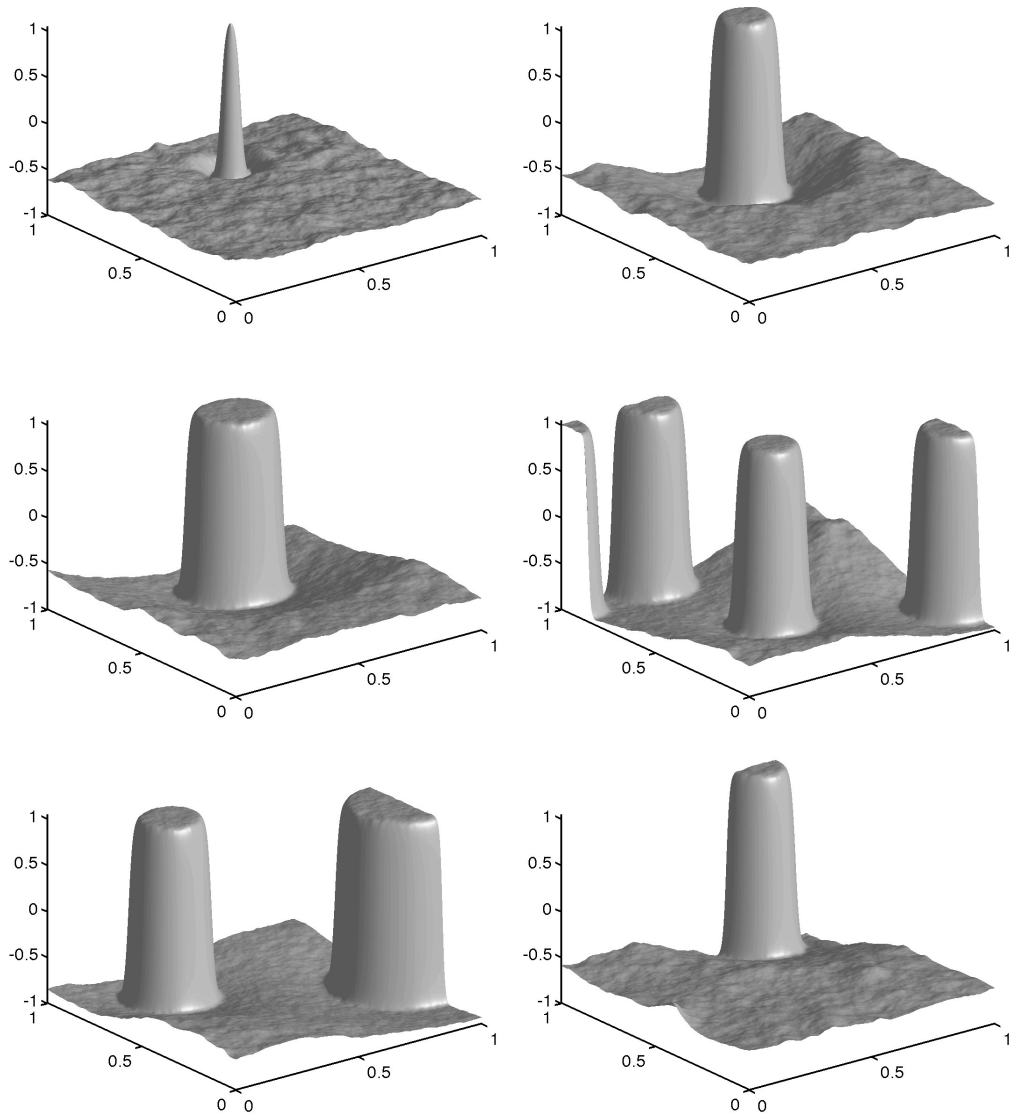

Figure 12: Snapshots of Cahn-Hilliard-Cook trajectories indicating nucleation behavior on the unit square $G = (0,1)^2$ with $\varepsilon = 0.01$, $\sigma_\varepsilon = 2$, and $m = -0.6$. The left column shows snapshots of one trajectory at times $t = 0.0628$, $t = 0.0942$, and $t = 0.1256$, from top to bottom. The right column shows nucleation morphologies generated by three additional, different trajectories.

Numerical results confirm this intuition. In the left column of Figure 12 we show solution snapshots of a trajectory $w(t)$ of (3) originating at $w(0) = m = -0.6$. After an initial period of small fluctuations around the homogeneous state, a droplet forms and subsequently grows. The actual growth dynamics after the initial droplet formation is reminiscent of the one-dimensional results in [3]. The center of the droplet increases to values close to $+1$; at the same time, on an annulus around the droplet center the values of w drop to -1. This initial phase separation is then followed by a growth phase of both the droplet and the region on which w is close to -1. While this simulation shows the formation of one droplet, other scenarios can be observed for different solution trajectories. Some of the resulting shapes of w are shown in the right column of Figure 12. These snapshots indicate that droplets can form at various positions in the base domain, even more or less simultaneously at different locations.

The few simulation results shown in Figure 12 already demonstrate that, at least from a qualitative point of view, the Cahn-Hilliard-Cook model is capable of intrinsically describing both the droplet formation and the subsequent dynamics. In [22] we performed a more extensive statistical study of nucleation dynamics in a multi-component version of (3). Using Monte Carlo type simulations for ternary alloys, we were able to derive distribution functions for quantities such as the time it takes for the first droplet to nucleate, or the position of the first droplet within the domain G. For more details, we refer the reader to [22].

From a mathematical point of view, the situation outlined so far is reminiscent of results due to Freidlin and Wentzell [29] in finite dimensions. They consider ordinary differential equations perturbed by additive white noise. In particular, they show that if the unperturbed deterministic equation has an attracting equilibrium $\bar{w}$, then with probability one, solutions of the stochastic equation originating at $\bar{w}$ leave any given bounded neighborhood of the equilibrium. Furthermore, for small intensities of the additive noise process they derive precise estimates for the exit time from the neighborhood, the most likely exit points, and the most likely exit paths. Finally, for the particular case of dissipative gradient systems, they relate the most likely exit points and the most likely exit paths to specific solutions of the unperturbed deterministic equation, i.e., to the structure of its global attractor. For more details we refer the reader to [29, Chapter 4]. Infinite-dimensional related results can be found in [11, 15, 20, 24, 59].

It seems that adapting the results of [29] to the Cahn-Hilliard-Cook model (3) can provide a complete and detailed description of nucleation, and preliminary results confirm this [8]. Yet, such results have to rely heavily on information concerning the attractor of the deterministic model (1). In this sense, a thorough understanding of both models is necessary to completely uncover their phase separation dynamics.

References

[1] R. A. Adams. Sobolev Spaces. Academic Press, San Diego – London, 1978.

[2] P. W. Bates, E. N. Dancer, and J. Shi. Multi-spike stationary solutions of the Cahn-Hilliard equation in higher-dimension and instability. *Advances in Differential Equations*, **4**(1):1–69, 1999.

[3] P. W. Bates and P. C. Fife. The dynamics of nucleation for the Cahn-Hilliard equation. *SIAM Journal on Applied Mathematics*, **53**(4):990–1008, 1993.

[4] P. W. Bates and G. Fusco. Equilibria with many nuclei for the Cahn-Hilliard equation. *Journal of Differential Equations*, **160**(2):283–356, 2000.

[5] P. W. Bates and G. Fusco. Multi-spike states of the Cahn-Hilliard model for phase transitions. In Concentration Phenomena in Elliptic and Parabolic Partial Differential Equations. Mathematical Society of Japan, to appear.

[6] D. Blömker. Stochastic Partial Differential Equations and Surface Growth. PhD thesis, Universität Augsburg, 2000.

[7] D. Blömker. Non-homogeneous noise and Q-Wiener processes on bounded domains. Stochastic Analysis and Applications, 2004. To appear.

[8] D. Blömker, B. Gawron, S. Maier-Paape, and T. Wanner. Work in progress.

[9] D. Blömker, S. Maier-Paape, and T. Wanner. Spinodal decomposition for the Cahn-Hilliard-Cook equation. *Communications in Mathematical Physics*, **223**(3):553–582, 2001.

[10] D. Blömker, S. Maier-Paape, and T. Wanner. Second phase spinodal decomposition for the Cahn-Hilliard-Cook equation. Submitted for publication, 2004.

[11] S. Brassesco. Some results on small random perturbations of an infinite-dimensional dynamical system. *Stochastic Processes and their Applications*, **38**(1):33–53, 1991.

[12] J. W. Cahn. Free energy of a nonuniform system. II. Thermodynamic basis. *Journal of Chemical Physics*, **30**:1121–1124, 1959.

[13] J. W. Cahn and J. E. Hilliard. Free energy of a nonuniform system I. Interfacial free energy. *Journal of Chemical Physics*, **28**:258–267, 1958.

[14] J. W. Cahn and J. E. Hilliard. Free energy of a nonuniform system III. Nucleation in a two-component incompressible fluid. *Journal of Chemical Physics*, **31**:688–699, 1959.

[15] M. Cassandro, E. Olivieri, and P. Picco. Small random perturbations of infinite-dimensional dynamical systems and nucleation theory. *Annales de l'Institut Henri Poincaré. Physique Théorique*, **44**(4):343–396, 1986.

[16] C. Conley. Isolated invariant sets and the Morse index. American Mathematical Society, Providence, R.I., 1978.

[17] H. Cook. Brownian motion in spinodal decomposition. *Acta Metallurgica*, **18**:297–306, 1970.

[18] R. Courant and D. Hilbert. *Methods of Mathematical Physics*. Intersciences, New York, 1953.

[19] G. Da Prato and A. Debussche. Stochastic Cahn-Hilliard equation. *Nonlinear Analysis. Theory, Methods & Applications*, **26**(2):241–263, 1996.

[20] G. Da Prato and J. Zabczyk. Stochastic Equations in Infinite Dimensions. Cambridge University Press, Cambridge, 1992.

[21] J. E. Deering. Computation of the bifurcation structure of the Cahn-Hilliard equation. Master's thesis, University of Maryland, Baltimore County, 2002.

[22] J. P. Desi and T. Wanner. The dynamics of nucleation in stochastic Cahn-Morral systems. In preparation, 2004.

[23] D. E. Edmunds and W. D. Evans. Spectral Theory and Differential Operators. Oxford University Press, Oxford – New York, 1987.

[24] W. G. Faris and G. Jona-Lasinio. Large fluctuations for a nonlinear heat equation with noise. *Journal of Physics A*, **15**(10):3025–3055, 1982.

[25] P. C. Fife. Models for phase separation and their mathematics. *Electronic Journal of Differential Equations*, 2000(48):1–26, 2000.

[26] P. C. Fife, H. Kielhöfer, S. Maier-Paape, and T. Wanner. Perturbation of doubly periodic solution branches with applications to the Cahn-Hilliard equation. *Physica D*, **100**(3–4):257–278, 1997.

[27] R. Franzosa. The connection matrix theory for Morse decompositions. *Transactions of the American Mathematical Society*, **311**(2):561–592, 1989.

[28] R. Franzosa and K. Mischaikow. Algebraic transition matrices in the Conley index theory. *Transactions of the American Mathematical Society*, **350**(3):889–912, 1998.

[29] M. I. Freidlin and A. D. Wentzell. Random Perturbations of Dynamical Systems. Springer-Verlag, New York, second edition, 1998.

[30] M. Gameiro, K. Mischaikow, and T. Wanner. Evolution of pattern complexity in the Cahn-Hilliard theory of phase separation. In preparation, 2004.

[31] C. P. Grant. Spinodal decomposition for the Cahn-Hilliard equation. *Communications in Partial Differential Equations*, **18**:453–490, 1993.

[32] M. Grinfeld and A. Novick-Cohen. Counting stationary solutions of the Cahn-Hilliard equation by transversality arguments. *Proceedings of the Royal Society of Edinburgh*, **125A**:351–370, 1995.

[33] M. Grinfeld and A. Novick-Cohen. The viscous Cahn-Hilliard equation: Morse decomposition and structure of the global attractor. *Transactions of the American Mathematical Society*, **351**(6):2375–2406, 1999.

[34] B. Hassard and J. Zhang. Existence of a homoclinic orbit of the Lorenz system by precise shooting. *SIAM Journal on Mathematical Analysis*, **25**(1):179–196, 1994.

[35] D. Henry. Geometric Theory of Semilinear Parabolic Equations, volume 840 of Lecture Notes in Mathematics. Springer-Verlag, Berlin – Heidelberg – New York, 1981.

[36] P. C. Hohenberg and B. I. Halperin. Theory of dynamic critical phenomena. *Reviews of Modern Physics*, **49**(3):435–479, 1977.

[37] J. M. Hyde, M. K. Miller, M. G. Hetherington, A. Cerezo, G. D. W. Smith, and C. M. Elliott. Spinodal decomposition in Fe-Cr alloys: Experimental study at the atomic level and comparison with computer models — II. Development of domain size and composition amplitude. *Acta Metallurgica et Materialia*, **43**:3403–3413, 1995.

[38] J. M. Hyde, M. K. Miller, M. G. Hetherington, A. Cerezo, G. D. W. Smith, and C. M. Elliott. Spinodal decomposition in Fe-Cr alloys: Experimental study at the atomic level and comparison with computer models — III. Development of morphology. *Acta Metallurgica et Materialia*, **43**:3415–3426, 1995.

[39] K. It$\bar{\text{o}}$. Foundations of stochastic differential equations in infinite-dimensional spaces, volume 47 of CBMS-NSF Regional Conference Series in Applied Mathematics. *Society for Industrial and Applied Mathematics* (SIAM), Philadelphia, PA, 1984.

[40] T. Kaczynski, K. Mischaikow, and M. Mrozek. Computational Homology, volume 157 of Applied Mathematical Sciences. Springer-Verlag, New York, 2004.

[41] H. Kielhöfer. Pattern formation of the stationary Cahn-Hilliard model. *Proceedings of the Royal Society of Edinburgh*, **127A**:1219–1243, 1997.

[42] H. Kielhöfer. Minimizing sequences selected via singular perturbations, and their pattern formation. *Archive for Rational Mechanics and Analysis*, **155**(4):261–276, 2000.

[43] J. S. Langer. Theory of spinodal decomposition in alloys. *Annals of Physics*, **65**: 53–86, 1971.

[44] S. Maier-Paape and U. Miller. Path-following the equilibria of the Cahn-Hilliard equation on the square. *Computing and Visualization in Science*, **5**(3):115–138, 2002.

[45] S. Maier-Paape, U. Miller, K. Mischaikow, and T. Wanner. Equilibria and attractor of the Cahn-Hilliard equation on the square. Submitted for publication, 2003.

[46] S. Maier-Paape, K. Mischaikow, and T. Wanner. Structure of the attractor of the Cahn-Hilliard equation on a square. In preparation, 2004.

[47] S. Maier-Paape and T. Wanner. Solutions of nonlinear planar elliptic problems with triangle symmetry. *Journal of Differential Equations*, **136**(1):1–34, 1997.

[48] S. Maier-Paape and T. Wanner. Spinodal decomposition for the Cahn-Hilliard equation in higher dimensions. Part I: Probability and wavelength estimate. *Communications in Mathematical Physics*, **195**(2):435–464, 1998.

[49] S. Maier-Paape and T. Wanner. Spinodal decomposition for the Cahn-Hilliard equation in higher dimensions: Nonlinear dynamics. *Archive for Rational Mechanics and Analysis*, **151**(3):187–219, 2000.

[50] M. K. Miller, J. M. Hyde, M. G. Hetherington, A. Cerezo, G. D. W. Smith, and C. M. Elliott. Spinodal decomposition in Fe-Cr alloys: Experimental study at the atomic level and comparison with computer models — I. Introduction and methodology. *Acta Metallurgica et Materialia*, **43**:3385–3401, 1995.

[51] K. Mischaikow. Conley index theory. In R. Johnson, editor, Dynamical Systems (Montecatini Terme, 1994), Lecture Notes in Mathematics 1609, pages 119–207. Springer-Verlag, Berlin – Heidelberg – New York, 1995.

[52] K. Mischaikow. Global asymptotic dynamics of gradient-like bistable equations. *SIAM Journal on Mathematical Analysis*, **26**:1199–1224, 1995.

[53] C. B. Muratov and E. Vanden-Eijnden. Breakup of universality in the generalized spinodal nucleation theory. Preprint, 2003.

[54] E.-M. Nash. Finite-Elemente und Spektral-Galerkin Verfahren zur numerischen Lösung der Cahn-Hilliard Gleichung und verwandter nichtlinearer Evolutionsgleichungen. PhD thesis, Universität Augsburg, 2000.

[55] B. Nicolaenko, B. Scheurer, and R. Temam. Some global dynamical properties of a class of pattern formation equations. *Communications in Partial Differential Equations*, **14**:245–297, 1989.

[56] A. Novick-Cohen. The Cahn-Hilliard equation: Mathematical and modeling perspectives. *Advances in Mathematical Sciences and Applications*, **8**(2):965–985, 1998.

[57] E. Sander and T. Wanner. Monte Carlo simulations for spinodal decomposition. *Journal of Statistical Physics*, **95**(5–6):925–948, 1999.

[58] E. Sander and T. Wanner. Unexpectedly linear behavior for the Cahn-Hilliard equation. *SIAM Journal on Applied Mathematics*, **60**(6):2182–2202, 2000.

[59] T. Shardlow. Nucleation of waves in excitable media by noise. Preprint, 2003.

[60] Z. Shi and B. Hassard. Precise solution of Laplace's equation. *Mathematics of Computation*, **64**(210):515–536, 1995.

[61] R. Temam. *Infinite-Dimensional Dynamical Systems in Mechanics and Physics*. Springer-Verlag, New York, second edition, 1997.

[62] H. Triebel. *Higher Analysis*. Johann Ambrosius Barth Verlag GmbH, Leipzig, 1992.

[63] J. D. van der Waals. The thermodynamic theory of capillarity flow under the hypothesis of a continuous variation in density. *Verh. Konink. Akad. Wetensch. Amsterdam*, **1**:1–56, 1893.

[64] J. B. Walsh. An introduction to stochastic partial differential equations. In *École d'été de probabilités de Saint-Flour, XIV—1984*, volume 1180 of *Lecture Notes in Math.*, pages 265–439. Springer, Berlin, 1986.

[65] T. Wanner. Maximum norms of random sums and transient pattern formation. *Transactions of the American Mathematical Society*, **356**(6):2251–2279, 2004.

[66] J. Wei and M. Winter. On the stationary Cahn-Hilliard equation: Interior spike solutions. *Journal of Differential Equations*, **148**(2):231–267, 1998.

[67] J. Wei and M. Winter. Stationary solutions for the Cahn-Hilliard equation. *Annales de l'Institut Henri Poincaré. Analyse Non Linéaire*, **15**(4):459–492, 1998.

[68] J. Wei and M. Winter. Multi-interior-spike solutions for the Cahn-Hilliard equation with arbitrarily many peaks. *Calculus of Variations and Partial Differential Equations*, **10**(3):249–289, 2000.

[69] P. Zgliczyński. Attracting fixed points for the Kuramoto-Sivashinsky equation: A computer assisted proof. *SIAM Journal on Applied Dynamical Systems*, **1**(2):215–235, 2002.

[70] P. Zgliczyński and K. Mischaikow. Rigorous numerics for partial differential equations: the Kuramoto-Sivashinsky equation. *Foundations of Computational Mathematics*, **1**(3):255–288, 2001.